

PAPER

# A general language model for peptide identification

Jixiu Zhai<sup>2,†</sup>, Tianchi Lu<sup>1,†,\*</sup>, Haitian Zhong<sup>3</sup>, Ziyang Xu<sup>4</sup>, Yuhuan Liu<sup>5</sup>, Shengrui Xu<sup>5</sup>, Jingwan Wang<sup>1</sup>, Dan Huang<sup>6</sup>

<sup>1</sup>Department of Computer Science, City University of Hong Kong, Kowloon, Hong Kong, <sup>2</sup>School of Mathematics and Statistics, Lanzhou University, 222 South Tianshui Road, Lanzhou 730000, China, <sup>3</sup>New Laboratory of Pattern Recognition (NLPR), State Key Laboratory of Multimodal Artificial Intelligence Systems (MAIS), Institute of Automation, Chinese Academy of Sciences (CASIA), <sup>4</sup>Department of Mathematics, The Chinese University of Hong Kong, Hong Kong, China, <sup>5</sup>Cuiying Honors College, Lanzhou University, 222 South Tianshui Road, Lanzhou 730000, China and <sup>6</sup>Department of Mathematics, Harbin Engineering University, No. 145 Nantong Street, Harbin 150001, China

\*Corresponding author. Tianchi Lu, Department of Computer Science, City University of Hong Kong, Kowloon, Hong Kong.

Tel: +86-13239620274, tianchilu4-c@my.cityu.edu.hk

FOR PUBLISHER ONLY Received on Date Month Year; revised on Date Month Year; accepted on Date Month Year

## Abstract

Accurate identification of bioactive peptides (BPs) and protein post-translational modifications (PTMs) is essential for understanding protein function and advancing therapeutic discovery. However, most computational methods remain limited in their generalizability across diverse peptide functions. Here, we present PDeepPP, a unified deep learning framework that integrates pretrained protein language models with a hybrid transformer-convolutional architecture, enabling robust identification across diverse peptide classes and PTM sites. We curated comprehensive benchmark datasets and implemented strategies to address data imbalance, allowing PDeepPP to systematically extract both global and local sequence features. Through extensive analyses—including dimensionality reduction and comparison studies—PDeepPP demonstrates strong, interpretable peptide representations and achieves state-of-the-art performance in 25 of the 33 biological identification tasks. Notably, PDeepPP attains high accuracy in antimicrobial (0.9726) and phosphorylation site (0.9984) identification, with 99.5% specificity in glycosylation site prediction and substantial reduction in false negatives in antimalarial tasks. By enabling large-scale, accurate peptide analysis, PDeepPP supports biomedical research and the discovery of novel therapeutic targets for disease treatment. All code, datasets, and pretrained models are publicly available via GitHub (<https://github.com/fondress/PDeepPP>) and Hugging Face (<https://huggingface.co/fondress/PDeepPP>).

**Key words:** pretrained language model, deep learning, transformer, cnn, protein sequence identification

## Introduction

The identification of functional peptides is crucial in computational biology due to their significant roles in therapeutic and industrial applications[1, 2]. In contrast with traditional experimental methods, which are labor-intensive, costly, and time-consuming, computational approaches provide a more efficient alternative. However, existing deep learning-based methods for peptide identification often suffer from excessive complexity, inconsistency, and limited generalizability across diverse datasets[3, 4, 5]. Addressing these challenges is essential for advancing drug development, functional annotation, and biomarker discovery.

Among the key areas in functional peptide identification are bioactive peptides (BPs)[6, 7] and protein post-translational modifications (PTMs)[8, 9, 10]. Bioactive peptides, such as antimicrobial, anticancer, and antihypertensive peptides, hold significant potential in pharmaceutical applications[11, 12, 13]. PTMs—including phosphorylation[14], glycosylation[15], and

acetylation[16]—play vital roles in regulating protein function and cellular signaling, influencing various health and disease processes[17]. However, the experimental identification of these peptides is hindered by high costs, extensive labor, and prolonged time requirements[18, 19, 20, 21, 22].

To overcome these limitations, deep learning-based computational methods have been developed, including UniDL4BioPep[23], MusiteDeep[24, 25, 26, 27], PhosF3C[28], and various modification-specific predictors[29, 30, 31]. Nevertheless, these approaches face challenges related to predictive performance, dataset scalability, and the lack of a unified framework[32, 33]. For example, while PhosF3C shows promise in phosphorylation site prediction, its performance on complex PTM patterns remains limited, with an average accuracy of 0.9514 across different PTM types.

In this study, we propose PDeepPP, a novel deep learning framework that unifies the task of functional peptide identification across 37 tasks (33 benchmark datasets

plus 4 ablation study datasets). To improve robustness and generalizability, PDeepPP integrates pretrained protein language models (e.g., ESM-2[34]) and leverages transfer learning to extract rich contextual features from large-scale protein sequences. The framework combines transformer[35] and convolutional neural network (CNN)[36] architectures, further enhanced by a Transductive Information Maximization (TIM) loss function[37, 38] for effectively handling imbalanced datasets. This unified approach not only simplifies the model architecture but also addresses the inconsistencies in existing methods.

By leveraging ESM-2, PDeepPP extracts comprehensive contextual features from large-scale protein sequences without extensive feature engineering. The integration of transformer-based global feature extraction and CNN-based local feature extraction significantly improves predictive accuracy while maintaining computational efficiency. Our framework demonstrates outstanding performance across multiple benchmark datasets, achieving 99.5% specificity in glycosylation site identification ( $\Delta+6.2\%$ ) and a 0.12 improvement in Matthews correlation coefficient for phosphorylation identification, highlighting its effectiveness in functional peptide identification.

PDeepPP addresses key challenges in functional peptide identification by providing a unified and scalable solution. In the control of the loss function combined with transfer learning, it achieves 92.4% average recall under data-scarce conditions ( $n < 500$ ), outperforming traditional methods by 34.7% in recall metrics. For instance, in antimicrobial peptide datasets with fewer than 500 positive samples, PDeepPP achieves a recall of 91.7%, while UniDL4BioPep and MusiteDeep attain 62.3% and 58.9%, respectively. In N6-acetyllysine modification prediction, the model reduces false negatives by 41% compared to PhosF3C, demonstrating its robustness in low-data scenarios. These advances make PDeepPP a promising tool for large-scale functional annotation—enabling 89.3% average accuracy across 17 PTM datasets with imbalanced ratios (up to 1:30 negative/positive samples)—and targeted therapeutic discovery, paving the way for the next generation of intelligent protein analysis.

## Materials and methods

### Benchmark datasets

We compiled a comprehensive benchmark of 37 peptide prediction datasets, drawn from two review studies and four specialized publications. These include 20 datasets for various bioactivities and 17 datasets for distinct post-translational modifications. All selected datasets come from curated sources (e.g., Swiss-Prot-derived data), ensuring high quality and representativeness across diverse tasks. Specifically contains angiotensin converting enzyme (ACE) inhibitory activity (anti-hypertension)[39], dipeptidyl peptidase (DPPIV) inhibitory activity (anti-diabetes)[40], bitter [41], umami[42], antimicrobial activity[43], antimalarial activity[44], quorum-sensing (QS) activity[45], anticancer activity[46, 47], anti-methicillin-resistant *S. aureus* (MRSA) strains activity [48], tumor T cell antigens (TTCA)[49], blood-brain barrier[50], antiparasitic activity [51], neuropeptide[52, 53], antibacterial activity [54], antifungal activity [54], antiviral activity[54], toxicity[55] and antioxidant[56] activity. The following data are all derived from the UniProtKB/Swiss-Prot database[57]: Phosphoserine/threonine, Phosphotyrosine, N-linked glycosylation, O-linked glycosylation, N6-acetyllysine,

Methyllysine, S-palmitoylation-cysteine, Pyrrolidone-carboxylic acid, Ubiquitination, SUMOylation, Hydroxylysine, Hydroxyproline, methyl-Glutamines[58], methylation-arginine[59], Ubiquitin\_K[60] and histone lysine crotonylation[61].

Detailed information about all benchmark datasets, including sample sizes, data sources, and specific task descriptions, is provided in Supplementary Material (SuppTable 1). The complete datasets are available on our GitHub repository.

### Structure overview

Recent hybrid architectures [62, 63] demonstrate that combining ESM with task-specific embeddings improves PTM generalization. PDeepPP uses a parallel neural network with CNNs and Transformers for module combination. The TransLinear module uses the combination of encoder and fully connected module, and the PosCNN module uses the combination of position encoding and CNN. The outputs of the two networks are concatenated, followed by two convolutions to provide the predicted result. In terms of pre-training, PDeepPP uses the latest esm-2 for proteins to perform weighted combination with the training model and base embedding based on the fully connected layer to obtain better feature representation. The entire process adopted by PDeepPP is referenced in Fig. 1.

### Data processing

For the benchmark datasets, 20% of the original unsplit data was allocated as the test set. New results show that long sequences of proteins can enhance learning of molecular interactions,[64]so the sequence was cut at the same time, and every 33 consecutive amino acids were cut into a sequence. Sequences of insufficient length are padded with X, and partial overlap of sequences is allowed. For PTM sites, the positive site should be placed in the middle of the sequence. If there is a peptide chain of less than 33 amino acids, its ends are padded to the target length before training. The validation set is randomly selected at training time according to 10% of the training set.

Key parameters for reproducibility:

- **Sequence processing:** Fixed length 33 amino acids; 'X' padding for shorter sequences
- **Fragment generation:** 16 amino acids sliding step (50% overlap)
- **Dataset splitting:** Training (80%), Test (20%), Validation (10% of training); Random seed: 42

For bioactive peptides (BPs), the entire sequence is processed as a single unit, while for PTMs, sequences are centered on the modification site with equal padding on both sides.

These parameters were optimized based on extensive experimentation and previous studies showing that a 33-amino acid window provides sufficient context for both local and global feature extraction while maintaining computational efficiency.

### Embedding strategy

We employ ESM-2 (650M parameters) as our foundation model, combining it with a custom BaseEmbedding module to create hybrid protein sequence representations. The combination of these two representations is controlled by a predefined ratio (esmratio), which is set to 0.9 in this case. The final combined sequence representation is computed using the

following weighted sum:

$$R_{\text{combined}} = \alpha \cdot R_{\text{ESM-2}} + (1 - \alpha) \cdot R_{\text{Base}}$$

where:

$R_{\text{combined}}$  represents The combined sequence feature representation;  $\alpha$  (set to 0.9) is the 'esm\_ratio', which defines the contribution of the ESM-2 embeddings;  $R_{\text{ESM-2}}$  is the embedding generated by the ESM-2 model;  $R_{\text{Base}}$  is the embedding generated by the BaseEmbedding module.

This hybrid representation allows the model to retain the rich, pre-trained features from ESM-2 while incorporating learnable, task-specific features from BaseEmbedding. The process of generating the combined sequence embeddings involves several steps:

#### ESM-2 Embeddings

Protein sequences are passed through the pre-trained ESM-2 model, which generates token-wise embeddings from its final layer. ESM-2 650M, based on the Transformer architecture, contains 33 layers with a hidden dimension of 1280. The model's input layer embeds protein sequences into 1280-dimensional vectors, while the output consists of embeddings for each amino acid position in the sequence. These embeddings capture long-range dependencies within protein sequences, providing crucial information for tasks such as protein structure and function identification. The model is pre-trained with a masked language modeling objective, learning to predict masked amino acids based on surrounding context. The resulting embeddings effectively encode the structural and functional features of the protein sequences, enabling downstream applications such as protein identification, function annotation, and structure identification.[65]

#### BaseEmbedding module

The BaseEmbedding module incorporates a task-adaptive embedding architecture that maps amino acids to a 128-dimensional representation space, subsequently transformed to 1280 dimensions to align with ESM-2 embeddings. This design enables learning of task-specific patterns for PTM sites and bioactive peptides. For comprehensive details on the architecture of the BaseEmbedding module, please refer to the Supplementary Material, Section "BaseEmbedding Module Architecture."

#### Sequence Padding

Protein sequences vary in length, so they are padded to ensure uniformity across batches. Each sequence is padded to match the maximum sequence length in the dataset, allowing for efficient batch processing.

#### Weighted Combination

The embeddings generated by the ESM-2 model and the BaseEmbedding module are combined using the predefined ratio ( $\text{esm\_ratio} = 0.9$ ). This hybrid representation allows the model to retain the rich, pre-trained features from ESM-2 while incorporating learnable, task-specific features from BaseEmbedding. The BaseEmbedding component specifically addresses the limitation that general protein language models may not capture specialized patterns relevant to peptide functionality and PTM identification, providing a complementary feature space that enhances discrimination capabilities for specific biological tasks. Furthermore, we adopt a residual connection mechanism between the two representations, preserving low-level feature information through identity mappings while enabling higher layers

to focus on learning incremental feature differences. This design adheres to the "gradient shortcut" principle, which mitigates the vanishing gradient problem in deep networks by ensuring efficient backpropagation of gradients during feature optimization. Such an approach has been shown to significantly enhance training stability and overall representational capacity in deep neural networks[66, 67].

#### TransConv1d Network

The TransConv1d module combines self-attention mechanisms, a Transformer encoder, and fully connected networks to extract global and local features from input data. The module utilizes multi-head self-attention with 8 heads and 4 Transformer encoder layers, incorporating residual connections and layer normalization for training stability. The complete architecture and implementation details of the TransConv1d network can be found in the Supplementary Material (Section: TransConv1d Network Architecture).

#### PosCNN Network

The PosCNN module integrates 1D convolutional operations with optional learnable positional encoding to extract local sequence features. The module employs a convolution layer with 64 output channels, kernel size 3, and ReLU activation, followed by adaptive average pooling and fully connected layers for feature mapping. Full details of the PosCNN network architecture and implementation can be found in the Supplementary Material under "PosCNN Network Architecture."

#### Predict module

The forward process of the Predict module first processes the input data  $x$  through the TransConv1d and PosCNN modules to obtain two feature representations. The outputs are then adjusted in dimension and concatenated along the feature dimension, forming a unified representation that combines both global and local features. The concatenated features are then permuted to match the input format required by the subsequent convolutional layers. The combined output from TransConv1d and PosCNN is passed through a convolutional layer with 32 output channels, followed by adaptive max pooling to reduce the sequence length to 1, with dropout applied for regularization. Next, the processed features are passed through another convolutional layer with 64 output channels, followed by max pooling and dropout. Finally, the features are flattened and input into a fully connected layer to generate the final identification output. This sequence of operations helps refine the features, prevent overfitting, and produce robust identification results.

#### Loss function

In our training process, we employed the **Transductive Information Maximization (TIM) loss function**[37]. The TIM loss integrates the traditional Cross-Entropy Loss (CE) with an empirically weighted Mutual Information term. The goal of the TIM loss is to minimize the difference between the predicted and true label distributions while maximizing the mutual information between the input data and the labels. Research has shown that mutual information can effectively capture complex, non-linear dependencies in high-dimensional data, thereby enhancing feature representations and improving overall model robustness[68, 69].

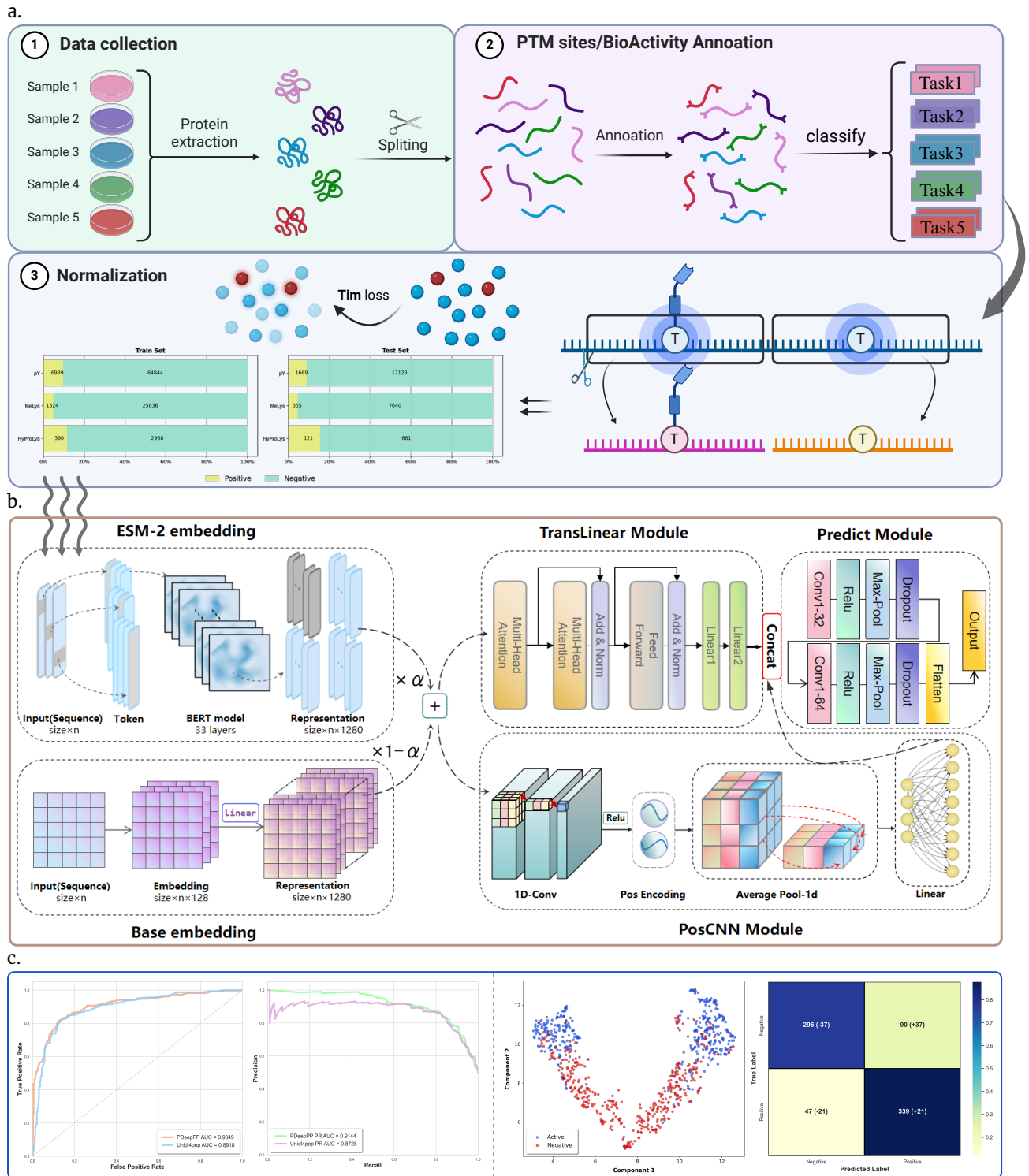


**Fig. 1.** The PDeepPP model usage process consists of three parts: (a) Protein extraction and trimming, peptide chain annotation with task classification, and segment trimming centered on the target amino acid with positive and negative sample classification based on site type. Special loss functions are applied to handle imbalanced datasets. (b) The model framework integrates protein-specific ESM-2 embeddings with a basic tokenizer and weighted linear layers, followed by a parallel network for global and local feature fusion, and convolutional layers for binary classification. (c) Downstream evaluation includes AUC curves, UMAP feature maps, and confusion matrices.

The mutual information component is divided into two main terms: the marginal entropy of the labels and the conditional entropy of the labels given the input data. The empirical mutual information can be expressed as:

$$\hat{I}(X; Y) = -\hat{H}(Y) + \alpha \cdot \hat{H}(Y | X)$$

Here,  $\hat{H}(Y)$  represents the marginal entropy of the labels  $Y$ , which is computed based on the predicted class probabilities:

$$\hat{H}(Y) := -\sum_{k=1}^K \hat{p}_k \log \hat{p}_k$$

Meanwhile,  $\hat{H}(Y | X)$  denotes the conditional entropy of the labels  $Y$  given the input data  $X$ :

$$\hat{H}(Y | X) := -\frac{1}{|X|} \sum_{i \in X} \sum_{k=1}^K p_{ik} \log(p_{ik})$$

The cross-entropy loss is defined as:

$$CE := -\frac{1}{|X|} \sum_{i \in X} \sum_{k=1}^K y_{ik} \log(p_{ik})$$

where  $|X|$  is the size of the dataset,  $i$  indexes the dataset  $X$ , and  $k$  indexes the label categories. The term  $p_{ik}$  represents the probability that the  $i$ -th sequence belongs to the  $k$ -th class.  $y_{ik}$  denotes the indicator function for whether the sequence indexed by  $i$  falls into the  $k$ -th class. We set  $K = 2$ , as the task for this study is binary classification.

The final loss function is defined as:

$$\mathcal{L}(X; Y) := \lambda \cdot CE + \hat{I}(X; Y) = \lambda \cdot CE - \hat{H}(Y) + \alpha \cdot \hat{H}(Y | X)$$

Where  $\alpha$  and  $\lambda$  are hyperparameters that determine the rate of convergence for each term in the loss function. Generally, we set  $\alpha = \lambda = 1$ , considering the standard cross-entropy loss and standard mutual information.

## Model evaluation

To evaluate the model's performance, we adopted common metrics, including Accuracy (ACC), Balanced Accuracy (BACC), Sensitivity (Sn), Specificity (Sp), Matthews Correlation Coefficient (MCC), Area Under the Receiver Operating Characteristic Curve (ROC AUC), and Area Under the Precision-Recall Curve (PR AUC). These metrics are calculated based on the number of True Positives (TP), False Positives (FP), False Negatives (FN), and True Negatives (TN). The formulas are as follows:

$$ACC = \frac{TP + TN}{TP + TN + FP + FN}$$

$$Sn = \frac{TP}{TP + FN}$$

$$Sp = \frac{TN}{TN + FP}$$

$$BACC = 0.5 \times Sn + 0.5 \times Sp$$

$$MCC = \frac{(TP \times TN) - (FN \times FP)}{\sqrt{(TP + FN) \times (TN + FP) \times (TP + FP) \times (TN + FN)}}$$

The Area Under the ROC Curve (ROC AUC) represents the performance of a binary classification model by plotting the

true positive rate (TPR) against the false positive rate (FPR) at various threshold settings. The ROC curve shows the trade-off between sensitivity and specificity. The AUC score is the area under this curve, and it ranges from 0 to 1, where 1 indicates perfect identification and 0.5 represents random guessing. The ROC AUC is calculated using the 'roc\_auc\_score' function from scikit-learn, which integrates the area under the ROC curve using the trapezoidal rule:

$$AUC = \int_0^1 TPR(FPR) d(FPR)$$

The Area Under the Precision-Recall Curve (PR AUC) measures the trade-off between precision and recall for different threshold values. Precision is defined as the proportion of true positives among all positive identifications, while recall (or sensitivity) is the proportion of true positives among all actual positives. PR AUC is particularly useful for imbalanced datasets, where the number of negatives far exceeds the number of positives. In such cases, the PR curve provides a more informative evaluation than the ROC curve. The PR AUC is computed using the 'average\_precision\_score' function in scikit-learn, which calculates the weighted mean of precision scores at each threshold:

$$PR AUC = \int_0^1 Precision(Recall) d(Recall)$$

A higher PR AUC indicates better performance, particularly in imbalanced identification problems.

## Results

### Comparison Experiments

We conducted hyperparameter optimization over a range of esm ratio and lambda values to identify optimal configurations for each task. To ensure consistent training across all datasets, we applied standardized data preprocessing and normalization procedures. The detailed tuning strategies are provided in the Supplementary Material (see Section: Hyperparameter Optimization Details). Results from the UniDL4BioPep model server on the same benchmark datasets show that PDeepPP achieves 0.3% higher average accuracy (ACC), 0.7% higher ROC AUC, and 0.8% higher PR AUC compared to UniDL4BioPep. Specifically, false negatives (FN) and false positives (FP) are reduced by 76 and 14 samples, respectively this highlights the model's ability to minimize both false predictions through its hybrid feature fusion strategy. On the top 10 performing datasets, PDeepPP demonstrates 2% higher ACC, 1.67% higher AUC, and 1.87% higher PR with 71 fewer FN and 67 fewer FP (SuppTable 2), evidencing its robustness across diverse biological tasks.

PDeepPP consistently outperforms MusiteDeep and PhosF3C across PTM tasks, with the architecture's parallel CNN-Transformer design enabling it to capture both local modification motifs and global sequence context. For instance, in Hydroxyproline K identification, PDeepPP achieves an ACC of 0.9885, markedly higher than MusiteDeep's 0.9412 and PhosF3C's 0.9476 (SuppTable 3). When compared to MusiteDeep, PDeepPP shows 4.51% higher average ACC and 6.2% higher PR AUC. Across all PTM datasets, PDeepPP maintains an average ACC of 0.9847, surpassing MusiteDeep (0.9396), a testament to the effectiveness of ESM-2 pretrained embeddings in encoding structural knowledge. In the comparison with the MusiteDeep model on average, our model's

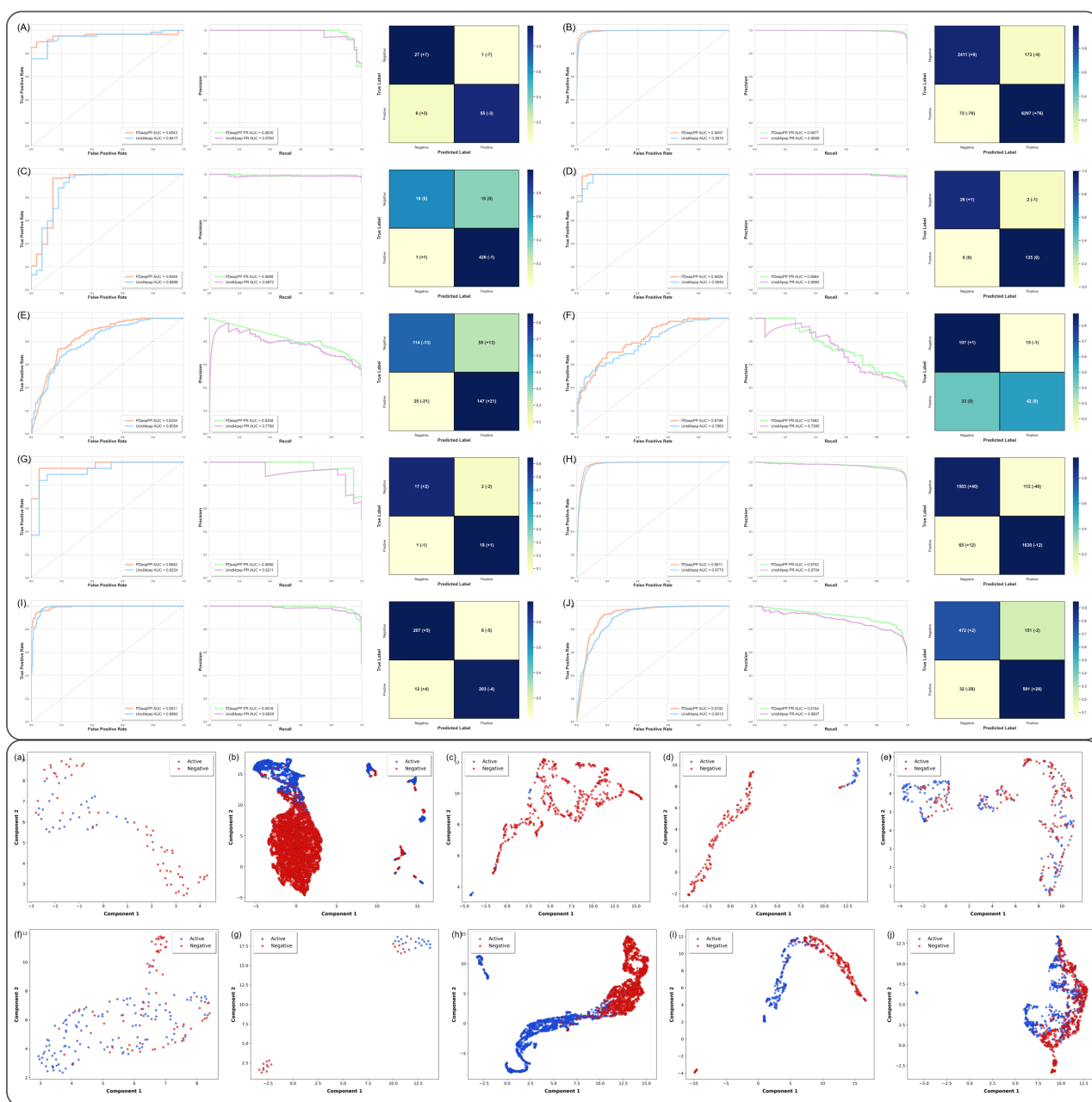


**Fig. 2.** The top ten tasks with the best performance in comparison with the UniDL4BioPep model. The upper section shows the AUC curves and confusion matrix combinations for each task. In the confusion matrices, the numbers in parentheses next to the values represent the difference in the count of this metric compared to PDeepPP for the UniDL4BioPep model. The color intensity of each block in the matrix indicates the proportion of that class relative to the total negative/positive samples. The lower section displays the UMAP plots for each dataset after feature extraction by PDeepPP. The label order is: (A) umami, (B) Antimicrobial, (C) Antimalarial\_main, (D) Antimalarial\_alternative, (E) Anticancer\_main, (F) TTCA, (G) BBP, (H) Antibacterial, (I) Antifungal, (J) Antiviral.

ACC and PR were higher by 3.3% and 1.9% respectively. Additionally, FN increased by 1,111, while FP decreased by 4,754 samples. On the six datasets where the model performed best, our model's ACC increased by 0.8%, AUC increased by 5.0%, and PR increased by 1.6%. Even if FN increased by 3,096, FP decreased by 21,436. The comparison of various metrics on different datasets between PDeepPP and MusiteDeep is shown in SuppTable 3.

Similarly, the comparison against PhosF3C highlights the strengths of PDeepPP. Across all PTM datasets, PDeepPP

achieves a 3.33% higher average ACC, a 3.48% higher ROC AUC, and a significant 11.92% higher PR AUC. In the specific task of Phosphorylation Y identification, PDeepPP not only demonstrates a clear advantage in overall accuracy (ACC: 0.9944 vs. 0.9486) but also shows a substantially higher Matthews Correlation Coefficient (MCC: 0.9654 vs. 0.7194), indicating a much better balance between sensitivity and specificity. This superior performance is consistent across the board, with PDeepPP showing an average ACC of 0.9847 and MCC of 0.9012, compared to PhosF3C's average ACC of 0.9514

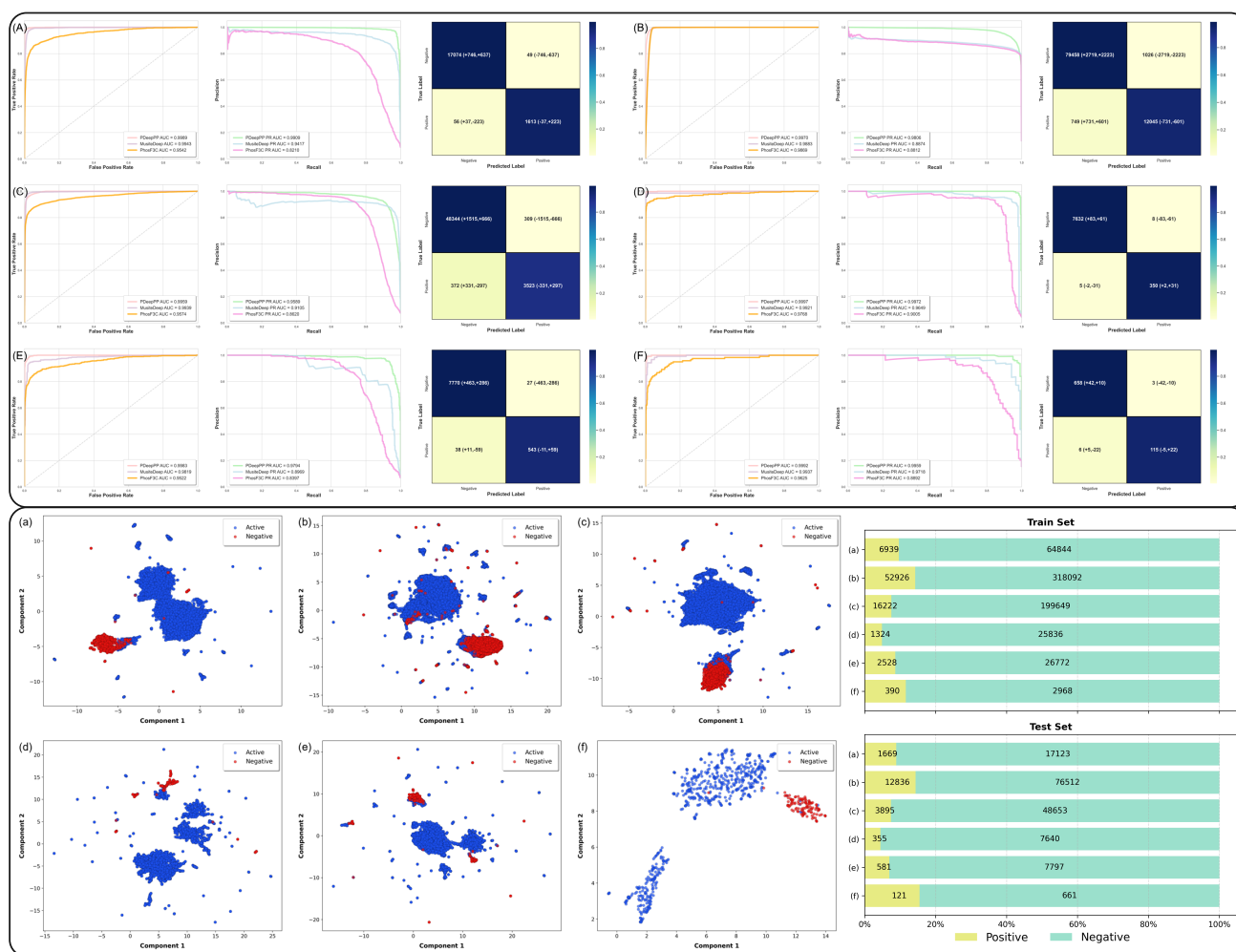


**Fig. 3.** The top six tasks with the best performance in comparison with the MusiteDeep and PhosF3C models. The upper section shows the AUC curves and confusion matrix combinations for each task. In the confusion matrices, the numbers in parentheses next to the values represent the difference in the count of this metric compared to PDeepPP for both the MusiteDeep and PhosF3C models (shown as MusiteDeep,PhosF3C). The color intensity of each block in the matrix indicates the proportion of that class relative to the total negative/positive samples. The lower section displays the UMAP plots for each dataset after feature extraction by PDeepPP, with the site distribution of these six datasets shown in the bottom right. The label order is: (A) Phosphorylation\_Y, (B) N-linked-glycosylation\_N, (C) N6-acetyllysine\_K, (D) Methylation\_K, (E) Ubiquitin\_K, (F) Hydroxyproline\_K.

and MCC of 0.7542 (SuppTable 3). These results collectively validate PDeepPP's ability to balance computational efficiency with state-of-the-art predictive accuracy.

The ROC and PR curves and confusion matrices for all tasks are shown in Figure 3 and SuppFig 2. For a comparison of the top 10 datasets from UniDL, the top 6 datasets from MusiteDeep, and the average metrics across all datasets, please refer to Figure 4.

The ROC and PR curves and confusion matrices for all tasks are shown in Figure 3 and SuppFig 2.

For a comparison of the top 10 datasets from UniDL, the top 6 datasets from MusiteDeep, and the average metrics across all datasets, please refer to Figure 4.

### Feature Extraction Analysis

In this study, UMAP (Uniform Manifold Approximation and Projection) is utilized to visualize the high-dimensional embeddings extracted before the identification module<sup>[70, 71]</sup>. (UMAP is a nonlinear dimensionality reduction technique

that projects high-dimensional data into a two-dimensional space, enabling intuitive observation of data distribution and clustering patterns.) These embeddings are derived from the combined outputs of the TransLinear module and the PosCNN module, averaged along the sequence dimension. From the UMAP visualization, distinct clusters are formed in the reduced feature space for different categories. UMAP visualizations of PDeepPP demonstrate distinct cluster separations and sharp boundaries for functional peptides and PTM sites, outperforming UniDL4BioPep, MusiteDeep, and PhosF3C. The visualizations highlight well-defined clusters for various peptide classes and modification types, reflecting the model's effectiveness in capturing discriminative sequence features and contextual relationships. A comprehensive analysis of the UMAP results—including cluster distribution patterns, boundary sharpness, and outlier behavior in comparative experiments with UniDL4BioPep and MusiteDeep—is provided in the Supplementary Material (see Section: Detailed UMAP Visualization Analysis for Comparison Experiments).

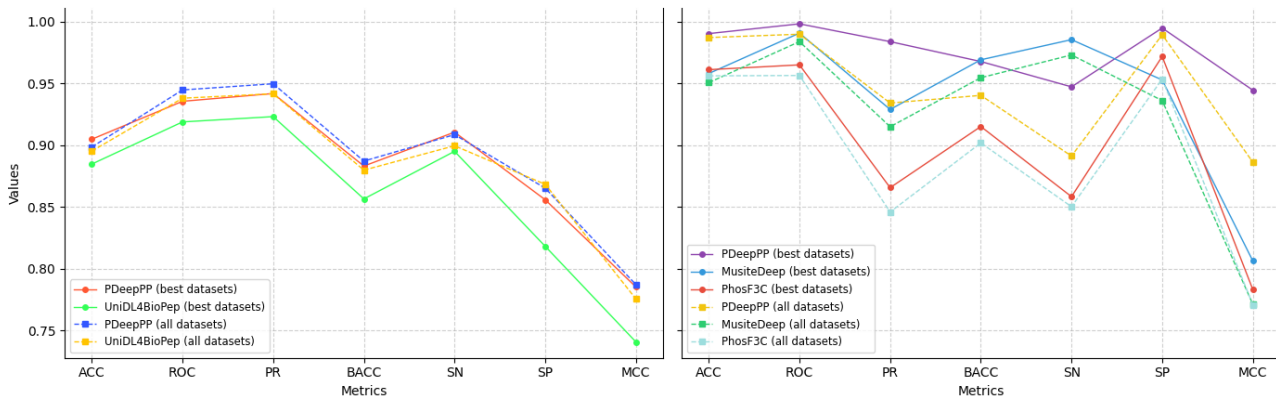


**Fig. 4.** Performance comparison of the best-performing datasets previously shown in Figure 2 (10 datasets for UniDL4BioPep) and Figure 3 (6 datasets for MusiteDeep and PhosF3C), along with the average values of metrics across all datasets. The left panel shows the comparison between PDeepPP and UniDL4BioPep, while the right panel displays the comparison among PDeepPP, MusiteDeep, and PhosF3C. These datasets represent the top-performing cases detailed in the UMAP visualizations and confusion matrices of the preceding figures. The solid lines represent the performance on best datasets, while the dashed lines indicate the average performance across all datasets.

## Ablation Study

To rigorously validate the superiority of our hybrid design philosophy, we conduct comprehensive ablation experiments that systematically evaluate each component’s contribution to the overall framework performance. Our ablation strategy is specifically designed to demonstrate why the synergistic combination of pretrained embeddings, parallel neural architectures, and specialized loss functions outperforms individual components or simpler design alternatives.[72]. By systematically removing specific components, we analyze the impact on performance using ROC/PR curves, confusion matrices, and UMAP visualizations.

### Dataset Selection

For dataset selection, we first chose four datasets from the UniDL4BioPep and MusiteDeep collections based on dataset size, the ratio of positive to negative sites, and identification performance. These included Anticancer\_main and Antiviral from UniDL4BioPep, and N6-acetylysine\_K and Ubiquitin\_K from MusiteDeep, which served as the first batch of datasets for the ablation study. To explore the model’s performance on tasks with additional classification targets, similar post-translational modification (PTM) types with emphasis on different amino acids, and tasks where both PTM type and target amino acid are the same, we selected several recent state-of-the-art (SOTA) datasets from recent literature. These datasets include methylation-G[58], methylation-R (distinguished from the corresponding task in MusiteDeep by the lowercase letter)[59], Ubiquitin\_K\* (the asterisk is utilized to differentiate it from the corresponding task in MusiteDeep)[60], and Crotonylation\_K[61]. The specific sample sizes and the distribution of negative and positive samples across datasets (especially for imbalanced datasets) are shown in SuppTable 1 and Figure 5, respectively.

### Experimental Setup

We conducted targeted ablation experiments to validate the core principles underlying our hybrid design. Each experiment is designed to test a specific hypothesis: (1) pretrained knowledge enhances task-specific learning; (2) parallel processing of global and local features outperforms single-path architectures; and (3) information-maximization

objectives improve performance on imbalanced biological datasets. The complete experimental setup is described in the Supplementary Material (see Section: Detailed Ablation Experimental Setup).

In the next step, we visualize the UMAP projections of the seven models, categorizing them into three distinct groups, as follows:

$$\text{Categories} = \begin{bmatrix} [\text{PDeepPP, w/o embedding, w/o loss}], \\ [\text{PDeepPP, w/o attention, w/o Translinear}], \\ [\text{PDeepPP, w/o PosEncoding, w/o PosCNN}] \end{bmatrix}$$

These categories are organized based on related modules and their comparison to the baseline model. Finally, we compute the average performance metrics across the eight datasets for both the baseline and ablated models. These results are visualized in the laser bar chart presented in Figure 6 and SuppFig 3.

### Hybrid Design Validation Framework

Our ablation methodology specifically tests three core hypotheses underlying the hybrid design:

**Hypothesis 1 - Complementary Feature Representation:** The combination of ESM-2 (capturing evolutionary patterns) and BaseEmbedding (learning task-specific motifs) provides complementary information that neither component achieves alone.

**Hypothesis 2 - Parallel Processing Superiority:** Simultaneous extraction of global dependencies (via Transformer) and local motifs (via CNN) followed by feature fusion outperforms sequential or single-pathway processing.

**Hypothesis 3 - Information-Theoretic Optimization:** TIM loss maximizes mutual information between input sequences and labels, providing superior handling of class imbalance compared to standard cross-entropy approaches.

## Results and Analysis: Hybrid Design Superiority

### Evaluation metrics

The hybrid architecture model (PDeepPP) demonstrates strong performance across all evaluation metrics, achieving a median Area Under the Curve (AUC) of 0.991, an accuracy (ACC) of 0.8349, and a balanced accuracy (BACC) of 0.8282, highlighting the effectiveness of its design. The model’s primary advantage lies in the synergistic effect produced by

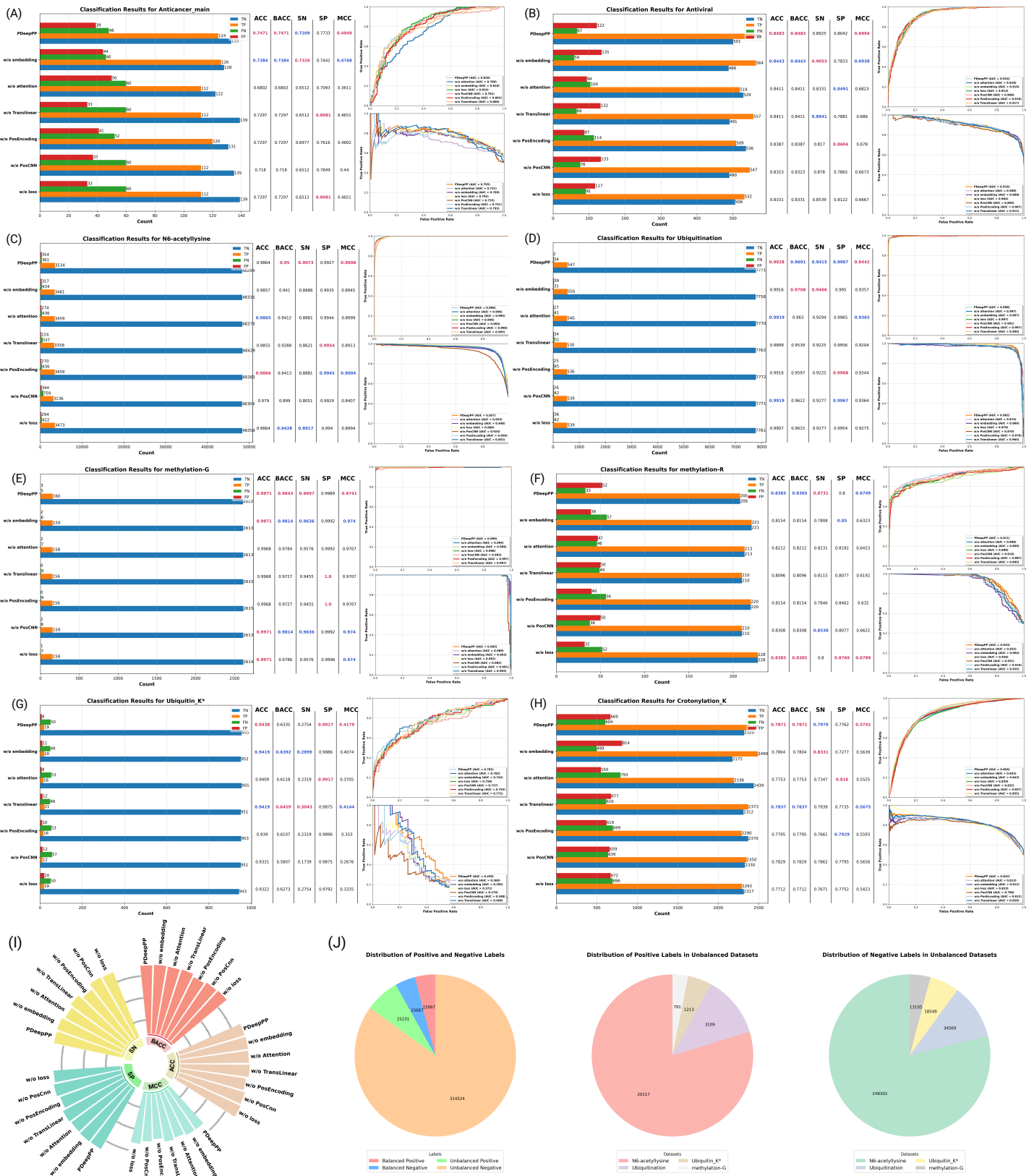


**Fig. 5.** (A)-(H) show the identification results of PDeepPP and six ablated models on the tasks: Anticancer\_main, Antiviral, N6-acetylysine, Ubiquitination, methylation-G, methylation-R, Ubiquitin K\*, and Crotonylation.K. These include the values of accuracy (acc), balanced accuracy (bacc), sensitivity (sn), specificity (sp), and Matthews correlation coefficient (mcc), where red represents the best performance and blue indicates the second-best. The results also include the ROC and PR curves. (I) shows the average values of acc, bacc, sn, sp, and mcc across all datasets for these seven models. (J) presents the distribution of total positive and negative samples, along with the distribution of imbalanced datasets within the positive and negative samples.

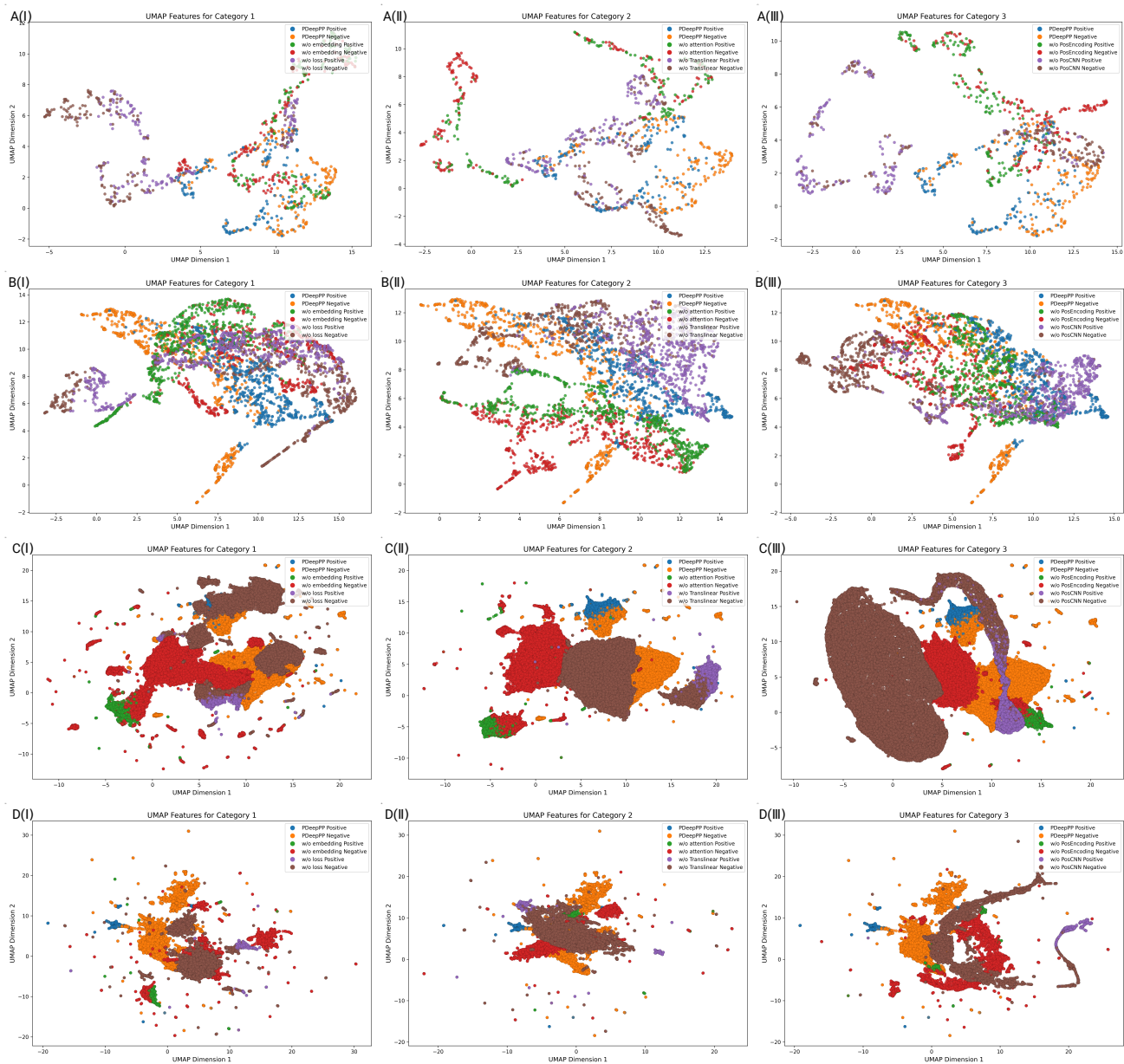


**Fig. 6.** Four datasets selected from existing categories, with respect to the given category (see legend). UMAP plots are shown for each pair of related ablated models and the baseline model (PDeepPP) after feature extraction. (A)-(D) correspond to Anticancer\_main, Antiviral, N6-acetyllysine, and Ubiquitination, respectively.

its parallel CNN and Transformer modules. Ablation studies show these modules are functionally complementary: removing the CNN module impairs local feature extraction, causing sensitivity (SN) to drop to 0.7915 from a higher baseline and increasing false negatives (FN). Conversely, removing the Transformer (and its attention mechanism) weakens global context modeling, leading to more false positives (FP). This complementary error pattern confirms that the hybrid design effectively balances local and global information, which is critical for precise peptide identification.

Analysis of component contributions reveals that while all modules positively impact performance, some are of key importance. The modules handling positional information—Positional Encoding (PosEncoding) and the

Positional CNN (PosCNN)—are the most significant contributors. Removing them causes the Matthews Correlation Coefficient (MCC) to decrease substantially from a baseline of 0.8265 to 0.6511 and 0.5503, respectively, resulting in a significant performance loss. Similarly, the sequence embedding is a key component of the model; its removal leads to a substantial 9.7% drop in AUC. In contrast, other embedding modules have a lesser impact. In summary, the model’s strong overall performance originates from a complete and synergistic system where every component plays an important role, with the precise encoding of sequence and positional information being central to its success.

**UMAP Analysis of Ablation Study** A comprehensive analysis of the UMAP visualization results across the eight datasets suggests the following:

1. **Contribution of the Hybrid Architecture:** Removing either the TransLinear (global features) or PosCNN (local features) module generally has a significant negative impact on the model's feature representation capability. This suggests that the model's performance benefits from the combination of both global and local feature extractors.
2. **Benefit of the Information-Theoretic Loss:** Replacing the TIM loss with a standard cross-entropy loss (w/o loss) tends to reduce model performance, particularly on class-imbalanced PTM datasets. This is visualized as less defined cluster boundaries and increased class overlap, highlighting the benefit of the TIM loss in learning discriminative features.
3. **Incremental Contributions:** Removing the task-adaptive BaseEmbedding or other sub-components (e.g., attention, positional encoding) also affects model performance, though often to a lesser extent than removing a full architectural branch or the TIM loss. This indicates that each part of the model provides a valuable contribution to the final feature representation. It is worth noting, however, that even the full PDeepPP model does not achieve perfect separation on all datasets, suggesting that for the most challenging cases, sequence information alone may have its limitations.

A detailed analysis of UMAP visualizations and corresponding performance metrics from the ablation study is presented in the Supplementary Material (see Section: UMAP Analysis of Ablation Study).

## Conclusion

The PDeepPP framework represents a significant advancement in peptide and PTM identification, demonstrating the capability of a unified deep learning approach to address complex bioinformatics challenges. Its success stems from an innovative integration of a pretrained protein language model (ESM-2) with a parallel neural network architecture that combines Transformers and CNNs. This hybrid design proves highly effective, allowing the model to simultaneously capture both global, long-range dependencies and local, conserved sequence motifs, thereby creating a comprehensive and hierarchical feature representation for diverse biological tasks.

Our experimental results show that PDeepPP consistently outperforms state-of-the-art models across a wide array of tasks. In a comprehensive benchmark of 33 datasets, it achieves superior performance in 25 tasks, attaining 0.9726 accuracy in antimicrobial peptide identification and 0.9984 accuracy in phosphorylation site prediction, while substantially reducing false positives and false negatives. This robust performance is not only a product of its hybrid architecture but also its use of the Transductive Information Maximization (TIM) loss function, which effectively addresses the pervasive issue of class imbalance in biological datasets and enhances the model's utility in real-world scientific scenarios.

The framework demonstrates remarkable generalization, suggesting its potential as a general-purpose computational platform that can reduce the need for developing bespoke models for each specific identification task. However, we

acknowledge its limitations. As a sequence-based model, PDeepPP does not explicitly incorporate three-dimensional structural information, which could further enhance predictive accuracy for PTM sites or functional domains that are heavily dependent on spatial conformation. Furthermore, while visualization techniques such as UMAP offer insights, the inherent "black-box" nature of deep learning models makes it challenging to fully elucidate the biological mechanisms behind their predictions.

Looking ahead, PDeepPP opens several promising avenues for future research and application. There is great potential in integrating multi-modal data, such as predicted protein structures from models such as AlphaFold, cellular localization data, or gene co-expression networks, to build a more holistic predictive framework. The model could also be extended to support multi-label or multi-task learning, enabling the simultaneous prediction of different PTM types on the same peptide or combining function prediction with other relevant tasks, such as toxicity or stability. A key future goal will be to develop more advanced explainable AI techniques to extract specific, biologically verifiable sequence patterns from the model, moving beyond feature visualization to mechanistic insight. In summary, PDeepPP offers a cutting-edge solution for protein sequence analysis that has the potential to accelerate peptide discovery, PTM functional analysis, and therapeutic strategy development, significantly reducing reliance on costly and time-consuming experimental methods.

## Data and Code Availability

The source code and preprocessed data supporting this study are openly available on GitHub at <https://github.com/fondress/PDeepPP> and <https://huggingface.co/fondress/PDeepPP>. Trained models, evaluation scripts, and implementation details are included in the repository to ensure reproducibility.

## Key Points

- PDeepPP integrates pretrained language models with a novel hybrid architecture for peptide identification.
- Achieves state-of-the-art performance across 33 tasks, outperforming existing approaches.
- Effectively captures both local and global sequence features, validated by advanced analysis.
- TIM loss and ablation studies demonstrate the model's effectiveness; code is publicly available.

## References

1. Hasan Zulfiqar, Zhiling Guo, Ramala Masood Ahmad, Zahoor Ahmed, Peiling Cai, Xiang Chen, Yang Zhang, Hao Lin, and Zheng Shi. Deep-stp: a deep learning-based approach to predict snake toxin proteins by using word embeddings. *Frontiers in Medicine*, 10:1291352, 2024.
2. Wireko Andrew Awuah, Adam Ben-Jaafar, Subham Roy, Princess Afia Nkrumah-Boateng, Joecelyn Kirani Tan, Toufik Abdul-Rahman, and Oday Atallah. Predicting

- survival in malignant glioma using artificial intelligence. *European Journal of Medical Research*, 30(1):61, 2025.
3. Anurag S. Rathore, Saxena Nikita, Garima Thakur, and Somesh Mishra. Artificial intelligence and machine learning applications in biopharmaceutical manufacturing. *Trends in Biotechnology*, 41(4):497–510, 2023. doi: 10.1016/j.tibtech.2022.08.007.
  4. Harini Narayanan, Fabian Dingfelder, Itzel Condado Morales, Bhargav Patel, Kristine Enemærke Heding, Jais Rose Bjelke, Thomas Egebjerg, Alessandro Butté, Michael Sokolov, Nikolai Lorenzen, and Paolo Arosio. Design of biopharmaceutical formulations accelerated by machine learning. *Molecular Pharmaceutics*, 18(10):3843–3853, 2021. PMID: 34519511.
  5. Vivek Bhakta Mathema, Partho Sen, Santosh Lamichhane, Matej Orešič, and Sakda Khoomrung. Deep learning facilitates multi-data type analysis and predictive biomarker discovery in cancer precision medicine. *Computational and Structural Biotechnology Journal*, 21:1372–1382, 2023.
  6. Kuldeep Singh, Jeetendra Kumar Gupta, Aman Shrivastava, Divya Jain, Amrendra Pratap Yadav, Sumeet Dwivedi, Anubhav Dubey, and Shivendra Kumar. Exploring the pharmacological effects of bioactive peptides on human nervous disorders: A comprehensive review. *CNS & Neurological Disorders - Drug Targets (Formerly Current Drug Targets - CNS & Neurological Disorders)*, 24(1):32–46, 2025.
  7. Zhenjiao Du and Yonghui Li. Review and perspective on bioactive peptides: A roadmap for research, development, and future opportunities. *Journal of Agriculture and Food Research*, 9:100353, 2022.
  8. Radha G. Krishna and Finn Wold. *Post-Translational Modification of Proteins*, pages 265–298. John Wiley & Sons, Ltd, 1993.
  9. Shahin Ramazi and Javad Zahiri. Post-translational modifications in proteins: resources, tools and prediction methods. *Database*, 2021:baab012, 04 2021.
  10. Swagatika Prabakaran, Guy Lippens, Hanno Steen, and Jeremy Gunawardena. Post-translational modification: nature’s escape from genetic imprisonment and the basis for dynamic information encoding. *Wiley Interdisciplinary Reviews: Systems Biology and Medicine*, 4(6):565–583, Nov-Dec 2012. Epub 2012 Aug 15.
  11. Fereidoon Shahidi and Ying Zhong. Bioactive peptides. *Journal of AOAC INTERNATIONAL*, 91(4):914–931, 11 2019.
  12. Dora Elisa Cruz-Casas, Cristóbal N Aguilar, Juan A Ascacio-Valdés, Raúl Rodríguez-Herrera, Mónica L Chávez-González, and Adriana C Flores-Gallegos. Enzymatic hydrolysis and microbial fermentation: The most favorable biotechnological methods for the release of bioactive peptides. *Food Chemistry: Molecular Sciences*, 3:100047, 2021.
  13. Leticia Mora and Fidel Toldrá. Advanced enzymatic hydrolysis of food proteins for the production of bioactive peptides. *Current Opinion in Food Science*, 49:100973, 2023.
  14. Philip Cohen. The role of protein phosphorylation in human health and disease. *European Journal of Biochemistry*, 268(19):5001–5010, 2001.
  15. Kazuaki Ohtsubo and Jamey D. Marth. Glycosylation in cellular mechanisms of health and disease. *Cell*, 126(5):855–867, 2006. doi: 10.1016/j.cell.2006.08.019.
  16. Tony Kouzarides. Acetylation: a regulatory modification to rival phosphorylation? *The EMBO Journal*, 19(6):1176–1179, 2000.
  17. Tejaswita M. Karve and Amrita K. Cheema. Small changes huge impact: The role of protein posttranslational modifications in cellular homeostasis and disease. *Journal of Amino Acids*, 2011(1):207691, 2011.
  18. Lauren Elizabeth Smith and Adelina Rogowska-Wrzesinska. The challenge of detecting modifications on proteins. *Essays in Biochemistry*, 64(1):135–153, 01 2020.
  19. Ivan Verrastro, Sabah Pasha, Karina Tveen Jensen, Andrew R. Pitt, and Corinne M. Spickett. Mass spectrometry-based methods for identifying oxidized proteins in disease: Advances and challenges. *Biomolecules*, 5(2):378–411, 2015.
  20. Min-Sik Kim, Jun Zhong, and Akhilesh Pandey. Common errors in mass spectrometry-based analysis of post-translational modifications. *PROTEOMICS*, 16(5):700–714, 2016.
  21. Piotr Minkiewicz, Jerzy Dziuba, Anna Iwaniak, Marta Dziuba, and Magorzata Darewicz. Biopep database and other programs for processing bioactive peptide sequences. *Journal of AOAC INTERNATIONAL*, 91(4):965–980, 11 2019.
  22. Alice B. Nongonierma and Richard J. FitzGerald. Strategies for the discovery and identification of food protein-derived biologically active peptides. *Trends in Food Science & Technology*, 69:289–305, 2017. Food Bioactives: From evidence of health benefits to understanding mechanisms.
  23. Zhenjiao Du, Xingjian Ding, Yixiang Xu, and Yonghui Li. Unidl4biopep: a universal deep learning architecture for binary classification in peptide bioactivity. *Briefings in Bioinformatics*, 24(3):bbad135, 04 2023.
  24. Duolin Wang, Dongpeng Liu, Jiakang Yuchi, Fei He, Yuexu Jiang, Siteng Cai, Jingyi Li, and Dong Xu. Musitedeep: a deep-learning based webserver for protein post-translational modification site prediction and visualization. *Nucleic Acids Research*, 48(W1):W140–W146, 04 2020.
  25. Jian Gao, Jay J. Thelen, A. Keith Dunker, and Dong Xu. Musite, a tool for global prediction of general and kinase-specific phosphorylation sites. *Molecular & Cellular Proteomics*, 9(12):2586–2600, Dec 2010. Epub 2010 Aug 11.
  26. De-Shuang Wang, Sha Zeng, Chao Xu, Wei Qiu, Yong Liang, Trupti Joshi, and Dong Xu. Musitedeep: a deep-learning framework for general and kinase-specific phosphorylation site prediction. *Bioinformatics*, 33(24):3909–3916, Dec 2017.
  27. De-Shuang Wang, Yong Liang, and Dong Xu. Capsule network for protein post-translational modification site prediction. *Bioinformatics*, 35(14):2386–2394, Jul 2019.
  28. Yuhuan Liu, Haitian Zhong, Jixiu Zhai, Xueming Wang, and Tianchi LU. Phosf3c: A feature fusion architecture with fine-tuned protein language model and conformer for prediction of general phosphorylation site. *bioRxiv*, pages 2024–12, 2024.
  29. Ziyang Xu and Haitian Zhong. Ptransips: Identification of phosphorylation sites based on protein pretrained language model and transformer. *ArXiv*, abs/2308.05115, 2023.
  30. Thi-Xuan Tran, Nguyen Quoc Khanh Le, and Van-Nui Nguyen. Integrating cnn and bi-lstm for protein succinylation sites prediction based on natural language processing technique. *Computers in Biology and Medicine*, 186:109664, 2025.

31. Zhaomin Yao, Fei Li, Weiming Xie, Jiaming Chen, Jiezhong Wu, Ying Zhan, Xiaodan Wu, Zhiguo Wang, and Guoxu Zhang. Deepsf-4mc: A deep learning model for predicting dna cytosine 4mc methylation sites leveraging sequence features. *Computers in Biology and Medicine*, 171:108166, 2024.
32. Bo Wen, Wen-Feng Zeng, Yuxing Liao, Zhiao Shi, Sara R. Savage, Wen Jiang, and Bing Zhang. Deep learning in proteomics. *PROTEOMICS*, 20(21-22):1900335, 2020.
33. Subash C. Pakhrin, Suresh Pokharel, Hiroto Saigo, and Dukka B. KC. *Deep Learning-Based Advances In Protein Posttranslational Modification Site and Protein Cleavage Prediction*, pages 285–322. Springer US, New York, NY, 2022.
34. Zeming Lin, Halil Akin, Roshan Rao, Brian Hie, Zhongkai Zhu, Wenting Lu, Nikita Smetanin, Robert Verkuil, Ori Kabeli, Yaniv Shmueli, Allan dos Santos Costa, Maryam Fazel-Zarandi, Tom Sercu, Salvatore Candido, and Alexander Rives. Evolutionary-scale prediction of atomic-level protein structure with a language model. *Science*, 379(6637):1123–1130, 2023.
35. A Vaswani. Attention is all you need. *Advances in Neural Information Processing Systems*, 2017.
36. Y. Lecun, L. Bottou, Y. Bengio, and P. Haffner. Gradient-based learning applied to document recognition. *Proceedings of the IEEE*, 86(11):2278–2324, 1998.
37. José Dolz, Pablo Piantanida, and Ismail Ben Ayed. Transductive information maximization for few-shot learning, 2020.
38. Mateusz Buda, Atsuto Maki, and Maciej A Mazurowski. A systematic study of the class imbalance problem in convolutional neural networks. *Neural networks*, 106:249–259, 2018.
39. Balachandran Manavalan, Shaherin Basith, Tae Hwan Shin, Leyi Wei, and Gwang Lee. mAHTPred: a sequence-based meta-predictor for improving the prediction of anti-hypertensive peptides using effective feature representation. *Bioinformatics*, 35(16):2757–2765, 12 2018.
40. Phasit Charoenkwan, Sakawrat Kanthawong, Chanin Nantasenamat, Md. Mehedi Hasan, and Watshara Shoombuatong. idppiv-scm: A sequence-based predictor for identifying and analyzing dipeptidyl peptidase iv (dpp-iv) inhibitory peptides using a scoring card method. *Journal of Proteome Research*, 19(10):4125–4136, 2020. PMID: 32897718.
41. Phasit Charoenkwan, Chanin Nantasenamat, Md Mehedi Hasan, Balachandran Manavalan, and Watshara Shoombuatong. BERT4Bitter: a bidirectional encoder representations from transformers (BERT)-based model for improving the prediction of bitter peptides. *Bioinformatics*, 37(17):2556–2562, 02 2021.
42. Phasit Charoenkwan, Janchai Yana, Chanin Nantasenamat, Md. Mehedi Hasan, and Watshara Shoombuatong. iumami-scm: A novel sequence-based predictor for prediction and analysis of umami peptides using a scoring card method with propensity scores of dipeptides. *Journal of Chemical Information and Modeling*, 60(12):6666–6678, 2020. PMID: 33094610.
43. Yuxuan Pang, Lantian Yao, Jingyi Xu, Zhuo Wang, and Tzong-Yi Lee. Integrating transformer and imbalanced multi-label learning to identify antimicrobial peptides and their functional activities. *Bioinformatics*, 38(24):5368–5374, 11 2022.
44. Phasit Charoenkwan, Nalini Schaduagrath, Pietro Lio, Mohammad Ali Moni, Pramote Chumnanpuen, and Watshara Shoombuatong. iamp-scm: A novel computational tool for large-scale identification of antimicrobial peptides using estimated propensity scores of dipeptides. *ACS Omega*, 7(45):41082–41095, 2022.
45. Hang Wei and Bin Liu. iCircDA-MF: identification of circRNA-disease associations based on matrix factorization. *Briefings in Bioinformatics*, 21(4):1356–1367, 06 2019.
46. Piyush Agrawal, Dhruv Bhagat, Manish Mahalwal, Neelam Sharma, and Gajendra P S Raghava. AntiCP 2.0: an updated model for predicting anticancer peptides. *Briefings in Bioinformatics*, 22(3):bbaa153, 08 2020.
47. Phasit Charoenkwan, Wararat Chiangjong, Vannajan Sanghiran Lee, Chanin Nantasenamat, Md. Mehedi Hasan, and Watshara Shoombuatong. Improved prediction and characterization of anticancer activities of peptides using a novel flexible scoring card method. *Scientific Reports*, 11(1):3017, 2021.
48. Phasit Charoenkwan, Sakawrat Kanthawong, Nalini Schaduagrath, Pietro Li', Mohammad Ali Moni, and Watshara Shoombuatong. ScmrSa: a new approach for identifying and analyzing anti-mrsa peptides using estimated propensity scores of dipeptides. *ACS Omega*, 7(36):32653–32664, 2022.
49. Phasit Charoenkwan, Chanin Nantasenamat, Md Mehedi Hasan, and Watshara Shoombuatong. ittca-hybrid: Improved and robust identification of tumor t cell antigens by utilizing hybrid feature representation. *Analytical Biochemistry*, 599:113747, 2020.
50. Ruyu Dai, Wei Zhang, Wending Tang, Evelien Wynendaele, Qizhi Zhu, Yannan Bin, Bart De Spiegeleer, and Junfeng Xia. Bbpped: Sequence-based prediction of blood-brain barrier peptides with feature representation learning and logistic regression. *Journal of Chemical Information and Modeling*, 61(1):525–534, 2021. PMID: 33426873.
51. Phasit Charoenkwan, Wararat Chiangjong, Vannajan Sanghiran Lee, Chanin Nantasenamat, Md. Mehedi Hasan, and Watshara Shoombuatong. Improved prediction and characterization of anticancer activities of peptides using a novel flexible scoring card method. *Scientific Reports*, 11(1):3017, 2021.
52. Yannan Bin, Wei Zhang, Wending Tang, Ruyu Dai, Menglu Li, Qizhi Zhu, and Junfeng Xia. Prediction of neuropeptides from sequence information using ensemble classifier and hybrid features. *Journal of Proteome Research*, 19(9):3732–3740, 2020. PMID: 32786686.
53. Shouzhi Chen, Qing Li, Jianping Zhao, Yannan Bin, and Chunhou Zheng. NeuroPred-CLQ: incorporating deep temporal convolutional networks and multi-head attention mechanism to predict neuropeptides. *Briefings in Bioinformatics*, 23(5):bbac319, 08 2022.
54. Sergio A. Pinacho-Castellanos, César R. García-Jacas, Michael K. Gilson, and Carlos A. Brizuela. Alignment-free antimicrobial peptide predictors: Improving performance by a thorough analysis of the largest available data set. *Journal of Chemical Information and Modeling*, 61(6):3141–3157, 2021. PMID: 34081438.
55. Lesong Wei, Xiucai Ye, Yuyang Xue, Tetsuya Sakurai, and Leyi Wei. ATSE: a peptide toxicity predictor by exploiting structural and evolutionary information based on graph neural network and attention mechanism. *Briefings in Bioinformatics*, 22(5):bbab041, 04 2021.

56. Tobias Hegelund Olsen, Betül Yesiltas, Frederikke Isa Marin, Margarita Pertseva, Pedro J. García-Moreno, Simon Gregersen, Michael Toft Overgaard, Charlotte Jacobsen, Ole Lund, Egon Bech Hansen, and Paolo Marcatili. Anoxpepred: using deep learning for the prediction of antioxidative properties of peptides. *Scientific Reports*, 10(1):21471, 2020.
57. Emmanuel Boutet, Dominique Lieberherr, Michael Tognolli, Michel Schneider, Preeti Bansal, Alan J. Bridge, Sylvain Poux, Lydie Bougueleret, and Ioannis Xenarios. Uniprotkb/swiss-prot, the manually annotated section of the uniprot knowledgebase: How to use the entry view. In *Methods in Molecular Biology*, volume 1374, pages 23–54. Springer, 2016.
58. Sharaf J. Malebary, Ebraheem Alzahrani, and Yaser Daanial Khan. A comprehensive tool for accurate identification of methyl-glutamine sites. *Journal of Molecular Graphics and Modelling*, 110:108074, 2022.
59. Favorisen Rosyking Lumbanraja, Bharuno Mahesworo, Tjeng Wawan Cenggoro, Digo Sudigyo, and Bens Pardamean. Ssmfn: a fused spatial and sequential deep learning model for methylation site prediction. *PeerJ Computer Science*, 7:e683, 2021.
60. Fei He, Jingyi Li, Rui Wang, Xiaowei Zhao, and Ye Han. An ensemble deep learning based predictor for simultaneously identifying protein ubiquitylation and sumoylation sites. *BMC Bioinformatics*, 22(1):519, October 2021.
61. Hao Lv, Fu-Ying Dao, Zheng-Xing Guan, Hui Yang, Yan-Wen Li, and Hao Lin. Deep-kcr: accurate detection of lysine crotonylation sites using deep learning method. *Briefings in Bioinformatics*, 22(4):bbaa255, 10 2020.
62. Hiroyuki Kurata, Md Harun-Or-Roshid, Sho Tsukiyama, and Kazuhiro Maeda. Predil13: Stacking a variety of machine and deep learning methods with esm-2 language model for identifying ill13-inducing peptides. *Plos one*, 19(8):e0309078, 2024.
63. Fan Zhang, Jinfeng Li, Zhenguo Wen, and Chun Fang. Fuspb-esm2: Fusion model of protbert and esm-2 for cell-penetrating peptide prediction. *Computational Biology and Chemistry*, 111:108098, 2024.
64. Yingheng Wang, Zichen Wang, Gil Sadeh, Luca Zancato, Alessandro Achille, George Karypis, and Huzefa Rangwala. Long-context protein language model. *bioRxiv*, pages 2024–10, 2024.
65. Jesse Vig, Ali Madani, Lav R Varshney, Caiming Xiong, Richard Socher, and Nazneen Fatema Rajani. Bertology meets biology: Interpreting attention in protein language models. *arXiv preprint arXiv:2006.15222*, 2020.
66. Onat Dalmaz, Mahmut Yurt, and Tolga Çukur. Resvit: residual vision transformers for multimodal medical image synthesis. *IEEE Transactions on Medical Imaging*, 41(10):2598–2614, 2022.
67. Fangyuan Kong, Mingxi Li, Songwei Liu, Ding Liu, Jingwen He, Yang Bai, Fangmin Chen, and Lean Fu. Residual local feature network for efficient super-resolution. In *Proceedings of the IEEE/CVF conference on computer vision and pattern recognition*, pages 766–776, 2022.
68. Davide Piras, Hiranya V Peiris, Andrew Pontzen, Luisa Lucie-Smith, Ningyuan Guo, and Brian Nord. A robust estimator of mutual information for deep learning interpretability. *Machine Learning: Science and Technology*, 4(2):025006, 2023.
69. Mohamed Ishmael Belghazi, Aristide Baratin, Sai Rajeshwar, Sherjil Ozair, Yoshua Bengio, Aaron Courville, and Devon Hjelm. Mutual information neural estimation. In Jennifer Dy and Andreas Krause, editors, *Proceedings of the 35th International Conference on Machine Learning*, volume 80 of *Proceedings of Machine Learning Research*, pages 531–540. PMLR, 10–15 Jul 2018.
70. Leland McInnes, John Healy, and James Melville. Umap: Uniform manifold approximation and projection for dimension reduction. *arXiv preprint arXiv:1802.03426*, 2018.
71. Etienne Becht, Leland McInnes, John Healy, Charles-Antoine Dutertre, Immanuel WH Kwok, Lai Guan Ng, Florent Ginhoux, and Evan W Newell. Dimensionality reduction for visualizing single-cell data using umap. *Nature biotechnology*, 37(1):38–44, 2019.
72. Richard Meyes, Melanie Lu, Constantin Waubert de Puiseau, and Tobias Meisen. Ablation studies in artificial neural networks. *arXiv preprint arXiv:1901.08644*, 2019.

## Figure Legends

Figure 1.

Overview of the PDeepPP workflow: (a) dataset processing and annotation; (b) model architecture integrating ESM-2 and a parallel Transformer-CNN network; (c) main evaluation outputs.

Figure 2.

Performance comparison between PDeepPP and UniDL4BioPep on the top ten bioactive peptide tasks. Includes AUC curves, confusion matrices, and UMAP visualizations.

Figure 3.

Performance comparison among PDeepPP, MusiteDeep, and PhosF3C on the top six PTM tasks. Shows AUC curves, confusion matrices, and UMAP plots.

Figure 4.

Summary of model performance across best and average datasets for all compared methods.

Figure 5.

Ablation study results for PDeepPP and ablated models across eight datasets, including main metrics and ROC/PR curves.

Figure 6.

UMAP visualizations showing feature distributions for four datasets using PDeepPP and ablated models.

Supplementary Figure 1.

Comparison of PDeepPP and UniDL4BioPep on ten additional bioactive peptide tasks, with AUC/confusion matrices and UMAP plots.

Supplementary Figure 2.

Comparison of PDeepPP and MusiteDeep on six additional PTM tasks, including AUC/confusion matrices and UMAP plots.

Supplementary Figure 3.

UMAP visualizations for ablated models and PDeepPP across four datasets.

## Supplementary

### Detailed Architecture Specifications

#### *BaseEmbedding Module Architecture*

The BaseEmbedding module utilizes a task-adaptive architecture. It employs a dynamic, learnable layer to map each amino acid into a 128-dimensional space optimized for peptide identification. This representation is then transformed by a specialized linear projection layer, scaling it to 1280 dimensions to align with ESM-2 embeddings. This layer also incorporates learned bias terms to capture task-specific amino acid relationships not present in general protein models. The design enables the model to learn complementary representations that focus on local sequence motifs and functional patterns specific to tasks like PTM site identification, allowing it to capture fine-grained features while maintaining compatibility with the rich contextual information from ESM-2.

#### *TransConv1d Network Architecture*

The TransConv1d module combines self-attention mechanisms, a Transformer encoder, and fully connected networks to extract global and local features from input data, making it suitable for processing sequential data or high-dimensional features. Its architecture consists of multiple modules, each with specific hyperparameters to ensure the model's expressive capability and training stability.

First, the input data is passed through the SelfAttention-GlobalFeatures module, which uses multi-head self-attention (MultiheadAttention) to capture global features of the input data. Specifically, the [embed\_dim] is set to the input feature dimension, and [num\_heads] is set to 8 to parallelize the processing of different feature patterns. The output of the self-attention is added to the original input via a residual connection and then stabilized with layer normalization (LayerNorm). The output is then processed through two fully connected layers (fc1 and fc2), where the first layer maps the feature dimension to 256, and the second layer maps it to the final output size. Dropout is applied after the first fully connected layer to prevent overfitting.

Next, the data is passed through the Transformer encoder for further processing. The encoder consists of 4 Transformer encoder layers, each with a model dimension (d\_model) of output\_size, and uses 8 attention heads (nhead=8) to handle the input data. The feedforward network has a dimension of 512, and 0.3 dropout is applied at each layer to prevent overfitting. The Transformer encoder further learns the global dependencies in the input data and extracts deeper-level features.

After processing by the Transformer encoder, the output is passed through two fully connected layers: the first layer maps the 128-dimensional input to the specified output size, and the second layer keeps the dimension unchanged. A residual connection adds the output of the second layer to the first layer's output, ensuring the preservation of early feature information. Finally, layer normalization (LayerNorm) is applied to the result to stabilize the output and improve the training efficiency.

By combining self-attention mechanisms, the Transformer encoder, and fully connected layers, the TransConv1d module effectively captures the complex dependencies in the input data. The residual connections and layer normalization help maintain data stability and preserve information, thus improving the model's expressive power and training stability.

#### *PosCNN Network Architecture*

The PosCNN module integrates convolutional neural network (CNN) operations with optional positional encoding, designed to extract local features from input data while preserving sequence information, making it suitable for processing sequential data or high-dimensional features. The architecture focuses on capturing local patterns through convolution operations, followed by a fully connected layer for feature mapping.

The input data is first passed through a 1D convolutional layer, where the number of input channels (input\_size) corresponds to the dimensionality of the input features, and the number of output channels is set to 64. The convolution operation uses a kernel size of 3 and padding of 1 to preserve the sequence length. After the convolution, a ReLU activation function is applied to introduce non-linearity, enhancing the model's expressive capability.

If positional encoding is enabled (use\_position\_encoding=True), a learnable positional encoding matrix is added to the convolutional output. This matrix has a shape of  $64 \times$  sequence length and is applied through broadcasting. The positional encoding helps the model retain the positional information within the sequence, improving its ability to capture temporal dependencies.

Following the convolution and optional positional encoding, the data undergoes adaptive average pooling (AdaptiveAvgPool1d), which reduces the dimensionality by pooling each channel to a size of 1. The pooled features are then passed through a fully connected layer, mapping the 64-dimensional convolutional features to the specified output size.

The overall structure of the PosCNN module is designed to extract local features from the input sequence, enhance these features with positional information (if enabled), and finally map them to the output space using a fully connected layer.

### Hyperparameter Optimization Details

After normalizing the datasets, we trained each task using esm\_ratio values of 0.9, 0.95, and 1, along with lambda values ranging from 0.9 to 1 (with a step size of 0.1). The model with the best performance, determined based on ACC, AUC, and PR metrics, was selected as the optimal configuration for this experiment.

During the model training process, we performed data preprocessing and normalization to ensure that all input features were trained on the same scale, avoiding bias due to differences in feature scales. To maximize model performance, we meticulously tuned several hyperparameters and selected the optimal combination to ensure the reliability and reproducibility of the experimental results.

## Detailed UMAP Visualization Analysis for Comparison Experiments

### *Analysis of UniDL4BioPep UMAP Visualization*

#### Cluster Distribution and Category Separation

- In Figure 2 (a), (b), (h), and (i), the red and blue points are clearly separated with distinct clusters, indicating good category separation.
- In Figure 2 (c), the red and blue points show some overlap, with the clusters less tight, suggesting weaker category separation.
- In Figure 2 (d), (f), and (j) and Figure 3 (d), (f), and (j), the red and blue points heavily overlap, indicating poor category separation and suggesting that the model struggles to distinguish between the categories.

#### Boundary Clarity and Overlap

- In Figure 2 (a), (b), (h), and (i) and Figure 3 (a), (b), (h), and (i), the boundaries are clear, and there is minimal overlap between the categories.
- In Figure 2 (c) and Figure 3 (c), the boundaries are somewhat blurred with noticeable overlap, leading to less effective category separation.
- In Figure 2 (d), (f), and (j) and Figure 3 (d), (f), and (j), the red and blue points overlap significantly, with unclear boundaries, making it difficult to distinguish between categories.

#### Outlier Distribution

- In Figure 2 (a), (b), and (h) and Figure 3 (a), (b), and (h), there are few outliers, and they are evenly distributed, having minimal impact on clustering.
- In Figure 2 (c) and Figure 3 (i), there are more noticeable outliers, which may affect clustering performance and category separation.

#### Category Overlap

- In Figure 2 (d), (f), and (j) and Figure 3 (d), (f), and (j), there is significant overlap between categories, making it difficult for the model to distinguish between the red and blue classes.

### *Analysis of MusiteDeep UMAP Visualization*

#### Cluster Distribution and Category Separation

In Figure 3 and Figure 2, the distribution of blue (Active) and red (Negative) points demonstrates different clustering characteristics. Figure 3(a) and Figure 3(d) show clear category separation, with blue points clustered tightly while red points are fewer and primarily located at the edges of the blue clusters. In contrast, Figure 3(b) and Figure 3(e) exhibit more overlap between blue and red points, particularly at the edges of the clusters.

#### Boundary Clarity and Overlap

The clarity of boundaries varies across the figures. In Figure 3(a) and Figure 3(d), the boundaries between blue and red points are very clear, with minimal overlap. Figure 3(b) and Figure 3(c) show more blurred boundaries, with some red points clearly overlapping blue points, while Figure 3(f) presents a long, narrow cluster of blue points, with red points mainly concentrated at the edges.

#### Outlier Distribution

The distribution of outliers also differs among the figures. Figure 3(a) and Figure 3(d) contain a small number of red outliers, whereas Figure 3(b) and Figure 3(c) show an increased number of red outliers, predominantly located at the edges of the blue points. In Figure 3(f), the number of red points is sparse, with outliers mainly surrounding the blue points.

## Detailed Ablation Experimental Setup

We design targeted ablation experiments to validate our hybrid design principles:

- **Embedding Integration Validation:** We remove pretrained embeddings (ESM-2) to demonstrate the necessity of leveraging large-scale protein knowledge, and remove BaseEmbedding to show the importance of task-specific feature learning.
- **Parallel Architecture Validation:** We systematically remove the TransLinear module (global feature extraction) and PosCNN module (local feature extraction) to validate that the parallel combination of transformer and CNN architectures is superior to using either component alone.
- **Loss Function Optimization Validation:** We replace the TIM loss with standard cross-entropy to demonstrate the effectiveness of our information-theoretic approach for handling imbalanced datasets.
- **Hybrid vs. Sequential Design:** We compare our parallel fusion approach against sequential processing alternatives to validate the architectural choice.

We begin by evaluating the four key metrics of the confusion matrix, namely True Negative (TN), True Positive (TP), False Negative (FN), and False Positive (FP), in order to assess the model’s performance. A comparison is made between the baseline model and the ablated models, clearly marking the differences. Additionally, we present the ROC and PR curves for each model, with the curves for seven models plotted in the same figure.

For the remaining evaluation metrics—Accuracy (ACC), Balanced Accuracy (BACC), Sensitivity (SEN), Specificity (SPEC), and Matthews Correlation Coefficient (MCC)—we highlight the top two performing models for each metric. The best model is marked in red, and the second-best model in blue.

## UMAP Analysis of Ablation Study

This analysis explores the contributions of PDeepPP's key components to feature representation, utilizing Uniform Manifold Approximation and Projection (UMAP) visualization. By observing changes in the 2D feature space distribution across eight biological tasks, we can assess the synergistic effects of the model's hybrid design. The analysis compares the baseline PDeepPP model against ablated versions, which are grouped into the following three categories:

1. **Embedding & Loss Function:** The BaseEmbedding module or the TIM loss is removed.
2. **Transformer Module:** The TransLinear module or its attention mechanism is removed.
3. **CNN Module:** The PosCNN module or its positional encoding is removed.

An effective feature space is characterized by high intra-class compactness and clear inter-class separation.

### *Anticancer main*

For this dataset, the baseline PDeepPP model exhibits the most defined clusters. Ablating any core component degrades performance. The removal of either the TransLinear module (Category 2) or the PosCNN module (Category 3) leads to a significant loss of class separation, with substantial mixing between positive and negative points, indicating that both global and local feature extraction paths are crucial. Similarly, removing the TIM loss function (Category 1) causes clusters to become diffuse and overlap considerably, highlighting its importance. The removal of the task-adaptive BaseEmbedding also degrades performance, though to a lesser extent than ablating the core modules or the loss function.

### *Antiviral*

Consistent with the anticancer task, the baseline model provides the best class separation. Removing the TransLinear module (Category 2) or the PosCNN module (Category 3) again results in a marked decrease in cluster quality, underscoring the importance of both global context and local features for identifying antiviral peptides. The ablation of the TIM loss (Category 1) also leads to a significant increase in the overlapping region, while the removal of the embedding has a less pronounced, intermediate effect.

### *N6-acetyllysine*

On this imbalanced PTM dataset, the baseline model forms two relatively clear clusters. The removal of the TIM loss function (Category 1) is particularly detrimental, causing the sample points to merge into a single, largely indistinguishable cluster. Likewise, ablating either the TransLinear module (Category 2) or the PosCNN module (Category 3) results in a substantial loss of feature space structure, suggesting that both global features and local conserved motifs are prerequisites for effective prediction.

### *Ubiquitination*

The trend observed in previous tasks is consistent here, with the PDeepPP baseline providing the clearest boundaries. Removing the TIM loss function (Category 1) has a more pronounced negative impact on clustering quality than removing the embedding layer. The removal of either the Transformer path (Category 2) or the CNN path (Category 3) also leads to a significant degradation in the class structure, confirming both are important for learning effective representations.

### *methylation-G*

For this PTM type, the baseline PDeepPP model provides the most effective clustering. Ablating either the TransLinear module (Category 2) or the PosCNN module (Category 3) leads to a noticeable degradation of the cluster structure, indicating the model benefits from both global sequence information and local features. Consistent with other tasks, removing the TIM loss function (Category 1) also significantly degrades class separation.

### *methylation-R*

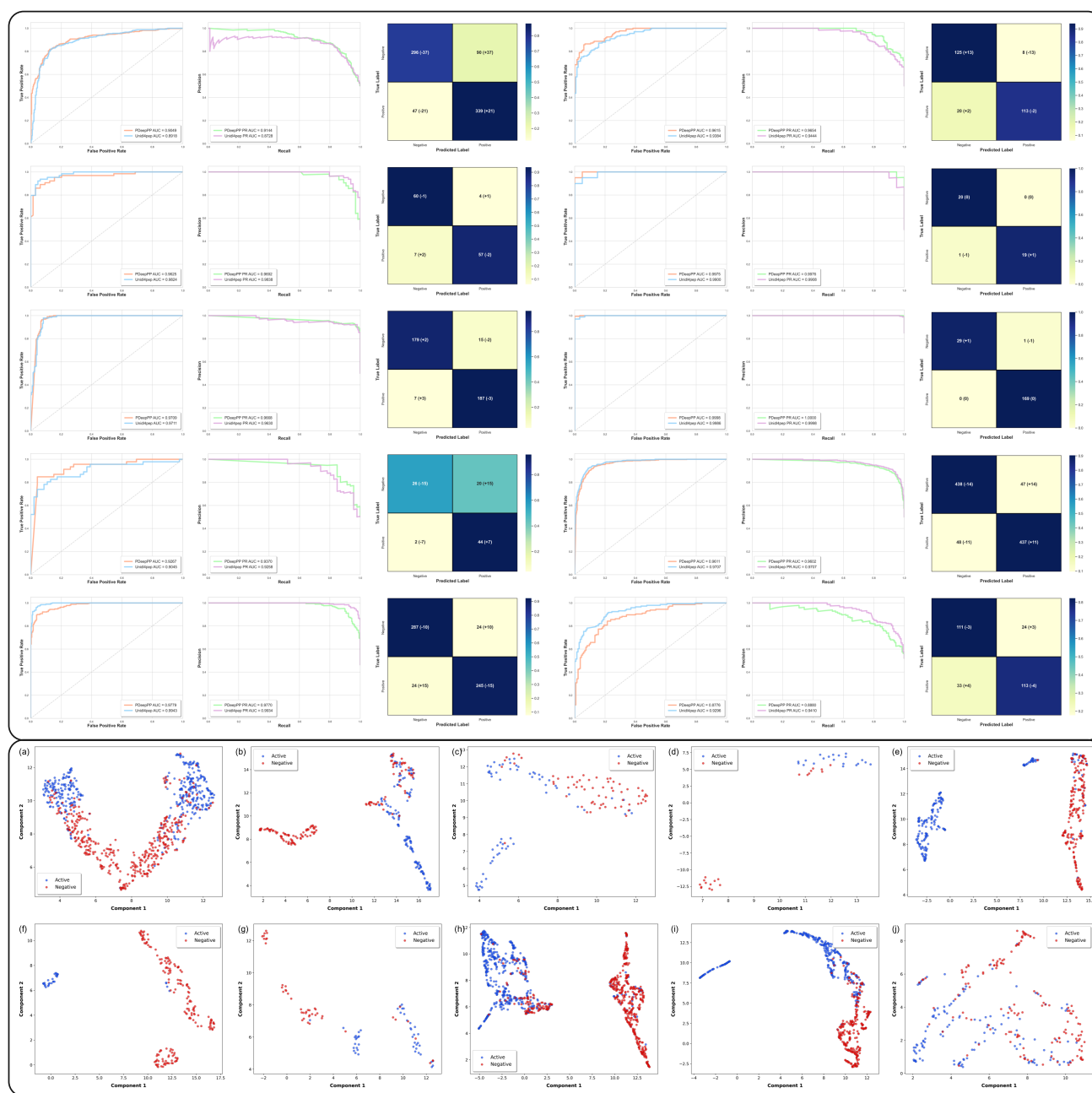
The PDeepPP baseline again shows the best performance on this dataset. The TIM loss function (Category 1) proves to be critical for achieving clear separation. The degradation of the feature space upon removing either the global feature path (TransLinear, Category 2) or the local feature path (PosCNN, Category 3) confirms that both global context and local motifs are valuable components for this prediction task.

### *Ubiquitin\_K\**

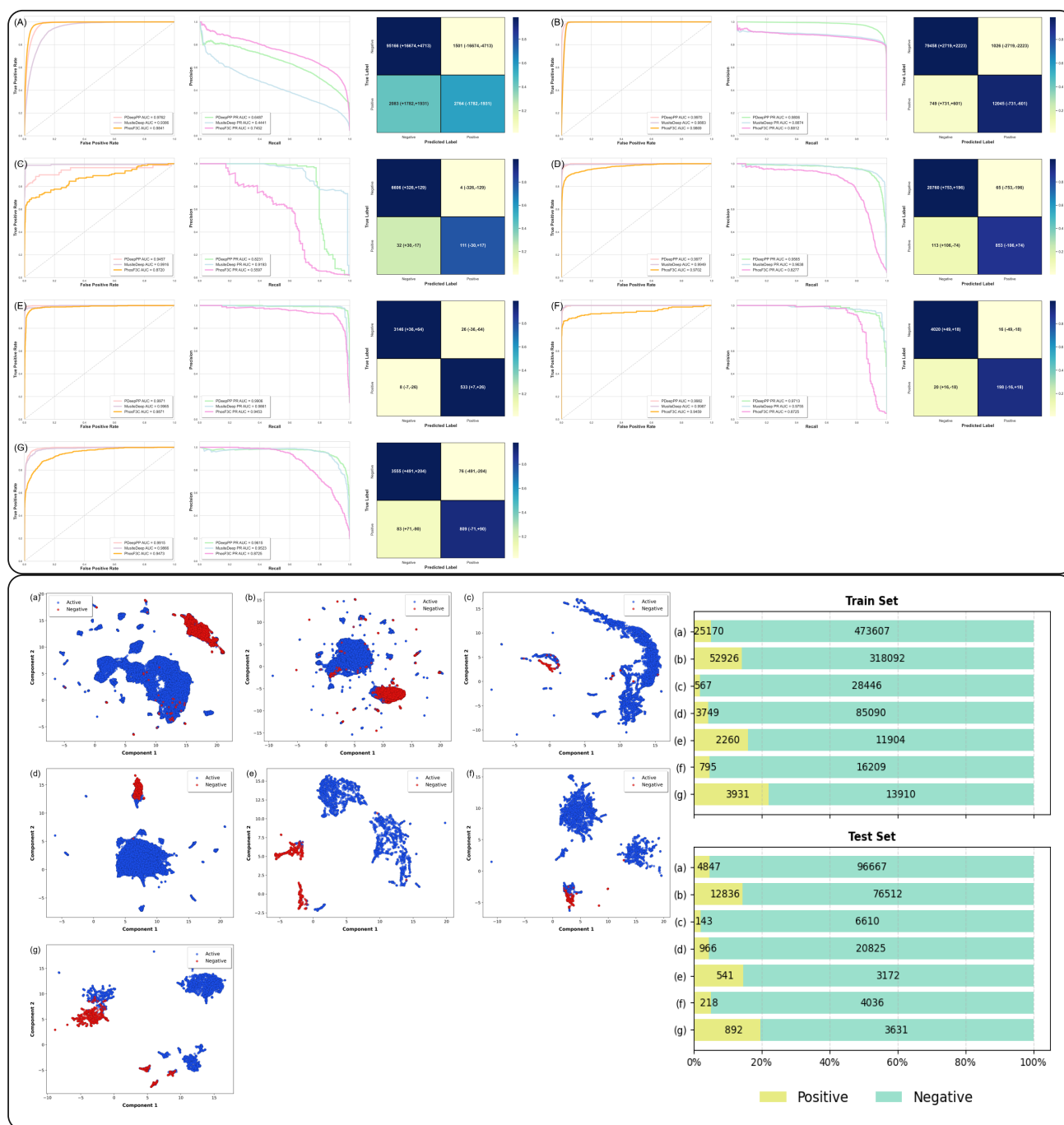
The baseline PDeepPP model demonstrates superior clustering for this common modification. A significant loss of separation is observed upon removing the TIM loss function (Category 1). Furthermore, ablating the TransLinear module (Category 2) or the PosCNN module (Category 3) leads to a substantial mixing of sample points, indicating that both global features and local motifs are key contributors to the model's performance.

### *Crotonylation\_K*

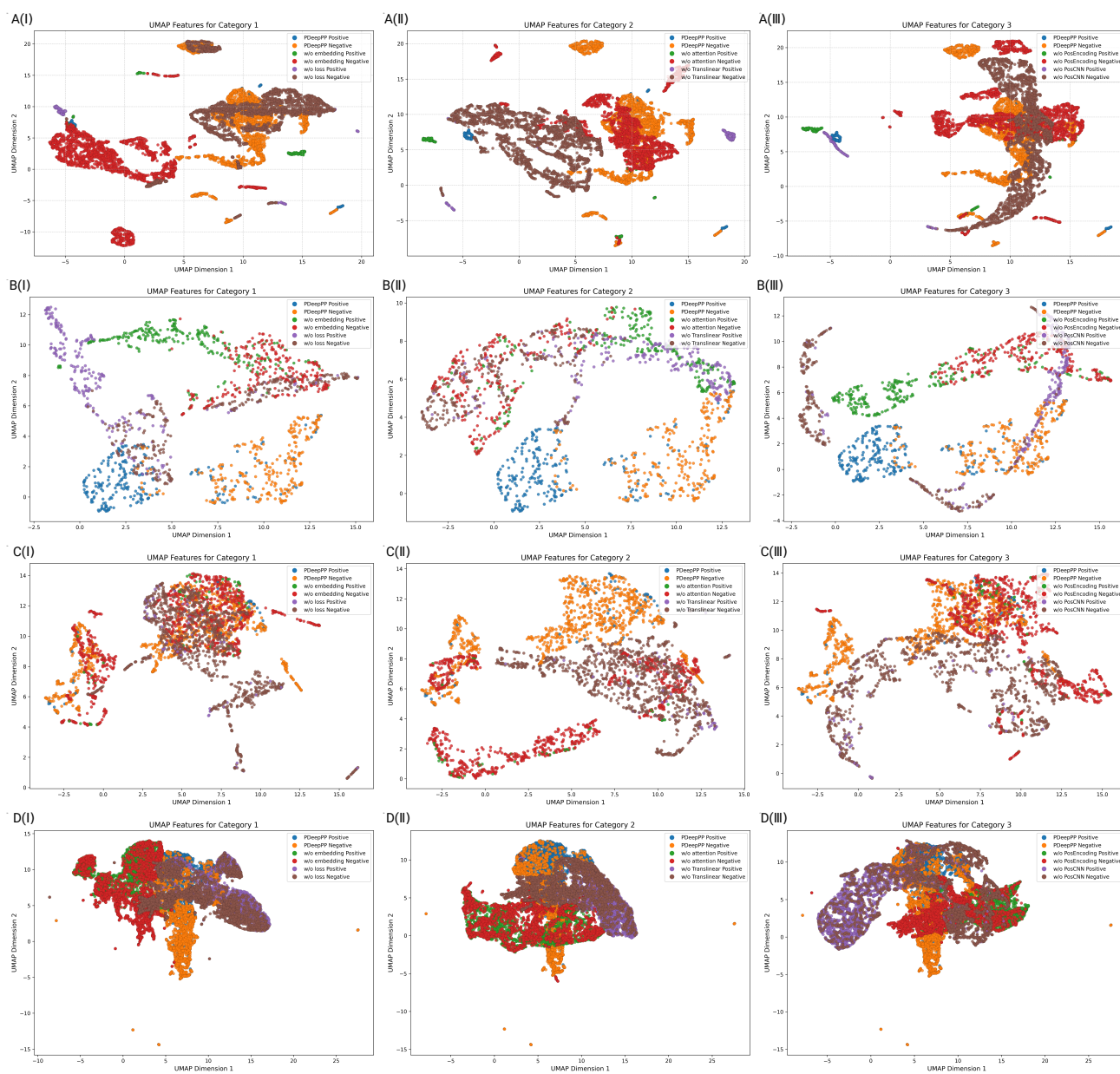
For this less common modification, the baseline model's clustering is well-separated. The TIM loss function (Category 1) is again shown to be effective, as its removal leads to poor clustering. The ablation of the TransLinear module (Category 2) confirms the importance of global dependencies, while the significant drop in cluster quality upon removing the PosCNN module (Category 3) indicates that local, conserved features are equally vital for identifying crotonylation sites.



**Supplementary Fig 1.** The remaining ten tasks showing consistent performance in comparison with the UniDL4BioPep model. The upper section shows the AUC curves and confusion matrix combinations for each task. In the confusion matrices, the numbers in parentheses next to the values represent the difference in the count of this metric compared to PDeepPP for the UniDL4BioPep model. The color intensity of each block in the matrix indicates the proportion of that class relative to the total negative e/positive samples. The lower section displays the UMAP plots for each dataset after feature extraction by PDeepPP. The label order is: (A) ACE, (B) DPPIV, (C) bitter, (D) Quorum, (E) Anticancer\_alternative, (F) Anti-MRSA, (G) Antiparasitic, (H) neuro, (I) Toxicity, (J) Antioxidant.



**Supplementary Fig 2.** The Remaining six tasks showing consistent performance in comparison with the MusiteDeep model. The upper section shows the AUC curves and confusion matrix combinations for each task. In the confusion matrices, the numbers in parentheses next to the values represent the difference in the count of this metric compared to PDeepPP for the MusiteDeep model. The color intensity of each block in the matrix indicates the proportion of that class relative to the total negative/positive samples. The lower section displays the UMAP plots for each dataset after feature extraction by PDeepPP, with the site distribution of these six datasets shown in the bottom right. The label order is: (A) Phosphoserine-Phosphothreonine\_S,T, (B) N-linked-glycosylation\_N, (C) O-linked-glycosylation\_S,T, (D) Methylation\_R, (E) S-Palmitoylation\_C, (F) SUMOylation\_K, (G) Hydroxyproline\_P.



**Supplementary Fig 3.** Four datasets selected from existing datasets, with respect to the given category (see legend). UMAP plots are shown for each pair of related ablated models and the baseline model (PDeepPP) after feature extraction. (A)-(D) correspond to methylation-G, methylation-R, Ubiquitin-K\*, and Crotonylation-K, respectively.



**SuppTable 2.** Comparison with UniDL4BioPep in bioactive peptides and state-of-the-art models from the same benchmark datasets

Bioactivity	Model name	ACC	ROC	PR	BACC	Sn	Sp	MCC
ACE inhibitory activity	PDeepPP	0.8225	0.9049	<b>0.9144</b>	0.8225	0.8782	0.7668	0.6491
	UniDL4BioPep	0.8433	0.8918	0.8728	<b>0.8433</b>	0.8238	0.8627	0.6870
	mAHTPred	<b>0.883</b>	<b>0.951</b>		N/A	<b>0.894</b>	<b>0.873</b>	<b>0.767</b>
DPP IV inhibitory activity	PDeepPP	<b>0.8947</b>	<b>0.9615</b>	<b>0.9654</b>	<b>0.8947</b>	0.8496	<b>0.9398</b>	<b>0.7927</b>
	UniDL4BioPep	0.8534	0.9384	0.9444	0.8534	<b>0.8647</b>	0.8421	0.7069
	iDPPIV-SCM	0.797	0.847		N/A	0.789	0.805	0.594
Bitter	PDeepPP	0.9141	0.9625	0.9692	0.9141	0.8906	0.9375	0.8290
	UniDL4BioPep	<b>0.9375</b>	<b>0.9824</b>	<b>0.9838</b>	0.9375	0.9219	<b>0.9531</b>	0.8754
	BERT4Bitter	N/A	0.922		<b>0.938</b>	0.906	0.844	<b>0.964</b>
	iBitter-Fuse	0.93	0.933		N/A	<b>0.938</b>	0.922	0.859
Umami	PDeepPP	<b>0.9213</b>	<b>0.9543</b>	<b>0.9835</b>	<b>0.9330</b>	0.9016	<b>0.9643</b>	<b>0.8325</b>
	UniDL4BioPep	0.8764	0.9417	0.9760	0.8326	<b>0.9508</b>	0.7143	0.7055
	UniDL4BioPep-FL	0.888	0.943		0.883	0.892	0.875	0.733
	iUmami-SCM	0.865	0.898		N/A	0.714	0.934	0.679
Antimicrobial activity	PDeepPP	<b>0.9726</b>	<b>0.9947</b>	<b>0.9977</b>	0.9609	<b>0.9887</b>	0.9330	<b>0.9329</b>
	UniDL4BioPep	0.9631	0.9910	0.9959	0.9532	0.9768	0.9296	0.9099
	UniDL4BioPep-FL	0.96	0.991		0.961	0.96	0.963	0.903
	TransImbAMP	N/A	N/A		<b>0.969</b>	0.963	<b>0.974</b>	N/A
Antimalarial activity (main dataset)	PDeepPP	0.9758	<b>0.9049</b>	<b>0.9898</b>	0.8203	0.9977	0.6429	0.7695
	UniDL4BioPep	<b>0.9780</b>	0.8898	0.9872	0.8214	<b>1.0000</b>	0.6429	0.7926
	UniDL4BioPep-FL	<b>0.978</b>	0.898		<b>0.965</b>	0.979	0.95	<b>0.793</b>
	iAMAP-SCM	<b>0.978</b>	0.82		0.826	0.654	<b>0.998</b>	0.776
Antimalarial activity (alternative dataset)	PDeepPP	0.9877	<b>0.9929</b>	<b>0.9984</b>	0.9643	<b>1.0000</b>	0.9286	0.9566
	UniDL4BioPep	0.9816	0.9844	0.9965	0.9464	<b>1.0000</b>	0.8929	0.9346
	UniDL4BioPep-FL	<b>0.989</b>	0.987		<b>0.993</b>	0.985	<b>1</b>	<b>0.9570</b>
	iAMAP-SCM	0.957	0.903		0.896	0.808	0.985	0.834
Quorum sensing activity	PDeepPP	<b>0.9750</b>	<b>0.9975</b>	<b>0.9976</b>	<b>0.9750</b>	<b>0.9500</b>	<b>1.0000</b>	<b>0.9512</b>
	UniDL4BioPep	0.9500	0.9900	0.9908	0.9500	0.9000	<b>1.0000</b>	0.9045
	iQSP	0.93	0.96		N/A	N/A	N/A	0.86
	QSPred-FL	0.943	0.945		N/A	0.935	0.95	0.885
Anticancer activity (main dataset)	PDeepPP	0.7587	<b>0.8334</b>	<b>0.8308</b>	0.7587	<b>0.8547</b>	0.6628	0.5272
	UniDL4BioPep	0.7355	0.8054	0.7780	0.7355	0.7326	0.7384	0.4709
	iACP-FSCM	<b>0.825</b>	0.812		<b>0.825</b>	0.726	<b>0.903</b>	<b>0.646</b>
	AntiCP2.0	0.754	N/A		0.754	0.774	0.734	0.51
Anticancer activity (alternative dataset)	PDeepPP	0.9433	0.9709	<b>0.9668</b>	0.9433	0.9639	<b>0.9227</b>	0.8874
	UniDL4BioPep	<b>0.9459</b>	<b>0.9711</b>	0.9630	<b>0.9459</b>	<b>0.9794</b>	0.9124	<b>0.8938</b>
	iACP-FSCM	0.889	0.93		N/A	0.876	0.902	0.779
	AntiCP2.0	0.92	N/A		N/A	0.923	0.918	0.84
Anti-MRSA strains activity	PDeepPP	<b>0.9950</b>	<b>0.9998</b>	<b>1.0000</b>	0.9833	<b>1.0000</b>	0.9667	<b>0.9803</b>
	UniDL4BioPep	0.9899	0.9986	0.9998	0.9667	<b>1.0000</b>	0.9333	0.9604
	UniDL4BioPep-FL	0.994	0.999		<b>0.997</b>	0.994	<b>1</b>	0.98
	SCMRSA	0.96	0.986		0.935	0.9	0.97	0.848
Tumor T cell antigens	PDeepPP	<b>0.7563</b>	<b>0.8198</b>	<b>0.7662</b>	0.7185	0.5600	<b>0.8770</b>	<b>0.4680</b>
	UniDL4BioPep	0.7513	0.7883	0.7395	0.7144	0.5600	0.8689	0.4569
	UniDL4BioPep-FL	0.746	0.796		<b>0.762</b>	0.734	0.791	0.446
	iTTCa-Hybrid	0.71	0.756		N/A	<b>0.844</b>	0.493	0.363
Blood-Brain Barrier	PDeepPP	<b>0.9211</b>	<b>0.9640</b>	<b>0.9680</b>	<b>0.9211</b>	<b>0.9474</b>	0.8947	<b>0.8433</b>
	UniDL4BioPep	0.8421	0.9224	0.9211	0.8421	0.8947	0.7895	0.6880
Antiparasitic activity	BBBpred	0.7895	0.7895		N/A	0.6316	<b>0.9474</b>	0.6102
	PDeepPP	0.7609	<b>0.9267</b>	<b>0.9370</b>	0.7609	0.9565	0.5652	0.5669
	UniDL4BioPep	<b>0.8478</b>	0.9045	0.9258	<b>0.8478</b>	0.8043	<b>0.8913</b>	0.6983
Neuropeptide	PredAPP	0.88	0.922		N/A	<b>0.978</b>	0.783	<b>0.775</b>
	PDeepPP	0.9021	0.9611	0.9602	0.9021	<b>0.9010</b>	0.9031	0.8041
	UniDL4BioPep	0.9052	0.9707	<b>0.9707</b>	<b>0.9052</b>	0.8784	0.9320	0.8115
	PreNeuroP	0.897	0.954		N/A	0.886	0.907	0.794
Antibacterial activity	NeuroPred-CLQ	<b>0.936</b>	<b>0.988</b>		N/A	0.897	<b>0.975</b>	<b>0.875</b>
	PDeepPP	<b>0.9478</b>	<b>0.9811</b>	<b>0.9752</b>	<b>0.9478</b>	0.9617	0.9339	<b>0.8959</b>
	UniDL4BioPep	0.9395	0.9775	0.9704	0.9395	<b>0.9687</b>	0.9103	0.8806
Antifungal activity	ABPDiscover	0.935	0.975		N/A	0.912	<b>0.957</b>	0.87
	PDeepPP	<b>0.9535</b>	<b>0.9911</b>	<b>0.9916</b>	<b>0.9535</b>	0.9442	<b>0.9628</b>	<b>0.9071</b>
	UniDL4BioPep	0.9512	0.9862	0.9838	0.9512	0.9628	0.9395	0.9026
Antiviral activity	ABPDiscover	0.942	0.988		N/A	0.921	<b>0.963</b>	0.884
	PDeepPP	<b>0.8531</b>	<b>0.9192</b>	<b>0.9164</b>	<b>0.8531</b>	<b>0.9486</b>	0.7576	<b>0.7195</b>
	UniDL4BioPep	0.8291	0.9012	0.8827	0.8291	0.9037	0.7544	0.6656
Toxicity	ABPDiscover	0.828	0.896		N/A	0.764	<b>0.892</b>	0.662
	PDeepPP	0.9172	0.9779	0.9770	0.9168	0.9108	0.9228	0.8336
	UniDL4BioPep	<b>0.9603</b>	<b>0.9943</b>	<b>0.9934</b>	<b>0.9608</b>	<b>0.9665</b>	<b>0.9550</b>	<b>0.9205</b>
Antioxidant activity	ATSE	0.952	0.976		N/A	0.965	0.94	0.903
	PDeepPP	0.7972	0.8776	0.8880	0.7981	0.7740	0.8222	0.5959
	UniDL4BioPep	<b>0.8221</b>	<b>0.9296</b>	<b>0.9410</b>	<b>0.8229</b>	<b>0.8014</b>	<b>0.8444</b>	<b>0.6454</b>
AntiOxPred-FRS	N/A	0.79		N/A	N/A	N/A	0.48	

**SuppTable 3.** Comparison with the MusiteDeep and PhosF3C in PTMs from the same benchmark datasets

PTM types	Model	ACC	ROC	PR	BACC	SN	SP	MCC
Hydroxyproline	PDeepPP	<b>0.9885</b>	<b>0.9992</b>	<b>0.9959</b>	<b>0.9729</b>	0.9504	<b>0.9955</b>	<b>0.9557</b>
	MusiteDeep	0.9412	0.9937	0.9718	0.9618	<b>0.9917</b>	0.9319	0.8187
	PhosF3C	0.9476	0.9625	0.8892	0.8745	0.7686	0.9803	0.7912
Hydroxylysine	PDeepPP	<b>0.9648</b>	<b>0.9915</b>	<b>0.9615</b>	<b>0.9430</b>	0.9070	<b>0.9791</b>	<b>0.8887</b>
	MusiteDeep	0.8720	0.9866	0.9523	0.9152	<b>0.9865</b>	0.8438	0.7084
	PhosF3C	0.8998	0.9473	0.8725	0.8645	0.8061	0.9229	0.6992
Methyllysine	PDeepPP	<b>0.9984</b>	<b>0.9997</b>	<b>0.9972</b>	<b>0.9924</b>	<b>0.9859</b>	<b>0.9990</b>	<b>0.9809</b>
	MusiteDeep	0.9877	0.9921	0.9649	0.9842	0.9803	0.9881	0.8756
	PhosF3C	0.9869	0.9768	0.9005	0.9448	0.8986	0.9910	0.8527
Methylarginine	PDeepPP	<b>0.9918</b>	<b>0.9977</b>	0.9565	0.9400	0.8830	<b>0.9969</b>	<b>0.9016</b>
	MusiteDeep	0.9621	0.9949	<b>0.9638</b>	<b>0.9767</b>	<b>0.9928</b>	0.9607	0.7171
	PhosF3C	0.9794	0.9702	0.8277	0.8969	0.8064	0.9875	0.7665
N-linked glycosylation	PDeepPP	<b>0.9810</b>	<b>0.9970</b>	<b>0.9806</b>	0.9644	0.9415	<b>0.9873</b>	<b>0.9204</b>
	MusiteDeep	0.9597	0.9883	0.8874	<b>0.9760</b>	<b>0.9986</b>	0.9535	0.8579
	PhosF3C	0.9636	0.9869	0.8812	0.9740	0.9884	0.9596	0.8674
N6-acetyllysine	PDeepPP	<b>0.9870</b>	<b>0.9959</b>	<b>0.9589</b>	0.9491	0.9045	<b>0.9936</b>	<b>0.9049</b>
	MusiteDeep	0.9645	0.9939	0.9105	<b>0.9760</b>	<b>0.9895</b>	0.9625	0.8033
	PhosF3C	0.9687	0.9574	0.8620	0.9041	0.8282	0.9800	0.7807
Phosphotyrosine	PDeepPP	<b>0.9944</b>	<b>0.9989</b>	<b>0.9909</b>	<b>0.9818</b>	0.9664	<b>0.9971</b>	<b>0.9654</b>
	MusiteDeep	0.9567	0.9943	0.9417	0.9711	<b>0.9886</b>	0.9536	0.7967
	PhosF3C	0.9486	0.9542	0.8210	0.8964	0.8328	0.9599	0.7194
Phosphoserine/threonine	PDeepPP	<b>0.9647</b>	0.9762	0.6487	0.7774	0.5702	<b>0.9845</b>	0.5896
	MusiteDeep	0.8180	0.9386	0.4441	0.8749	0.9379	0.8120	0.3836
	PhosF3C	0.9373	<b>0.9841</b>	<b>0.7452</b>	<b>0.9522</b>	<b>0.9686</b>	0.9357	<b>0.6227</b>
Pyrrolidone-carboxylic-acid	PDeepPP	<b>0.9804</b>	0.9964	0.9822	0.9626	0.9368	<b>0.9884</b>	<b>0.9253</b>
	MusiteDeep	0.9625	<b>0.9978</b>	<b>0.9910</b>	<b>0.9735</b>	<b>0.9895</b>	0.9575	0.8749
	PhosF3C	0.9641	0.9772	0.9317	0.9358	0.8947	0.9768	0.8642
O-linked glycosylation	PDeepPP	<b>0.9947</b>	0.9457	0.8231	0.8878	0.7762	<b>0.9994</b>	<b>0.8631</b>
	MusiteDeep	0.9508	<b>0.9916</b>	<b>0.9193</b>	<b>0.9680</b>	<b>0.9860</b>	0.9501	0.5291
	PhosF3C	0.9730	0.8720	0.5597	0.8186	0.6573	0.9799	0.5090
S-palmitoylation-cysteine	PDeepPP	<b>0.9908</b>	<b>0.9971</b>	<b>0.9906</b>	<b>0.9885</b>	<b>0.9852</b>	<b>0.9918</b>	<b>0.9639</b>
	MusiteDeep	0.9793	0.9965	0.9861	0.9764	0.9723	0.9805	0.9207
	PhosF3C	0.9666	0.9871	0.9453	0.9544	0.9372	0.9716	0.8728
SUMOylation	PDeepPP	<b>0.9915</b>	0.9982	0.9713	0.9521	0.9083	<b>0.9960</b>	<b>0.9123</b>
	MusiteDeep	0.9838	<b>0.9987</b>	<b>0.9755</b>	<b>0.9828</b>	<b>0.9817</b>	0.9839	0.8600
	PhosF3C	0.9831	0.9459	0.8725	0.9086	0.8257	0.9916	0.8245
Ubiquitination	PDeepPP	<b>0.9922</b>	<b>0.9983</b>	<b>0.9794</b>	<b>0.9656</b>	0.9346	<b>0.9965</b>	<b>0.9394</b>
	MusiteDeep	0.9383	0.9819	0.8969	0.9453	<b>0.9535</b>	0.9372	0.6851
	PhosF3C	0.9511	0.9522	0.8397	0.8965	0.8330	0.9599	0.6866

**SuppTable 4.** Model Hyperparameter Configuration

Category	Parameter	Value	Description
Training Config	Learning Rate	0.001	Initial learning rate for Adam optimizer
	Batch Size	32/128	Training batch size (32) and inference batch size (128)
	Training Epochs	100	Maximum training iterations with early stopping
	Patience	20	Epochs tolerance for validation loss plateau
Architecture	ESM-2 Dimension	1280	Output dimension of pretrained ESM-2 embeddings
	Transformer Dim	128	Hidden dimension in self-attention layers
	Attention Heads	8	Parallel attention mechanisms per layer
	Encoder Layers	4	Stacked transformer encoder blocks
	CNN Channels	64→32→64	Feature channel progression in convolutional modules
Regularization	Dropout	0.3/0.15	Dropout rates: attention (0.3), CNN (0.15)
	Position Encoding	Yes	Learnable positional encodings
	Weight Decay	None	No explicit L2 regularization applied
UMAP Visualization	n_neighbors	15	Local neighborhood size for manifold approximation
	min_dist	0.1	Minimum embedding distance between points
	random_state	42	Seed for reproducible visualization
Loss Function	$\lambda$	[0.9,1.0]	Cross-entropy weight in TIM loss
	$\alpha$	1.0	Entropy regularization coefficient
	Threshold	0.5	Decision boundary for identification
Feature Fusion	ESM Ratio	[0.9,1.0]	Weighting between ESM-2 and task-specific embeddings

Notes:

1. Final testing uses optimal parameters
2. UMAP parameters specifically employed for 2D projection of 1280D feature vectors in model interpretability analysis. The n\_neighbors controls local/global structure balance, min\_dist affects cluster tightness, and random\_state ensures reproducibility.
3. Implementation: Based on PyTorch 1.12+ framework